Two Dimensional Normal Modes in Arbitrary Enclosed Basins on a Rotating Earth: Application to Lakes Ontario and Superior

D. B. Rao and D. J. Schwab

Email alerting service	Receive free email alerts when new articles cite this article - sign up in the box at the top right-hand corner of the article or click **here**

TWO DIMENSIONAL NORMAL MODES IN ARBITRARY ENCLOSED BASINS ON A ROTATING EARTH: APPLICATION TO LAKES ONTARIO AND SUPERIOR

By D. B. RAO† AND D. J. SCHWAB†

Department of Energetics, and Center for Great Lakes Studies,
The University of Wisconsin–Milwaukee, U.S.A.‡

CONTENTS

A method for determining the free periods of oscillation of an arbitrary enclosed homogeneous water body on a rotating earth is considered. Bathymetry and shape of the water body are taken into account. The oscillations are quasi-static and horizontally two dimensional. Analytical foundation of the theory is based upon a method developed by Proudman (1916). The method requires the construction of two sets of orthogonal functions; one set satisfies a condition of vanishing normal derivative on the boundary and the other set of functions have a zero value on the boundary. These orthogonal functions are numerically constructed for two real water bodies. The numerical ortho-gonal functions are used as a basis for the expansion of velocity and height fields. The expansion coefficients are then determined so as to satisfy the dynamical equations. The coefficients appear as eigenvectors of a Hermitian matrix. The corresponding

† Present address: National Oceanic and Atmospheric Administration, Great Lakes Environmental Research Laboratory, Ann Arbor, Michigan, 48104.
‡ Contribution no. 139.

eigenvalues represent the frequencies of oscillation. Structures are determined by numerical evaluation of the velocity and height field expansions.

Application of the above procedure to Lake Ontario gives for the lowest gravitational mode a period of 5.11 h and for Lake Superior, the period of the corresponding mode is 7.86 h. Periods of the lowest six gravitational modes and their structures in both lakes are presented. Comparison of Lake Superior calculations with the data analysis of Mortimer & Fee (1976, preceding paper) shows very good agreement. A few examples of rotational modes are also presented.

1. INTRODUCTION

The free oscillations of a homogeneous water body with variable depth on a rotating plane consist of two distinct types referred to as gravitational modes (oscillations of the first class) and rotational modes (oscillations of the second class). Gravitational modes, produced by undulations of the free surface of a homogeneous fluid, generally have frequencies (σ) larger than the local Coriolis parameter f.[†] Existence of these modes is in no way related to the Earth's rotation. The rotation has only a modifying influence on the properties of the gravitational modes. Rotational modes, on the other hand, correspond to low frequency oscillations with $\sigma < f$. The generation of rotational modes depends on the existence of a gradient of potential vorticity in the basic state of fluid configuration. The potential vorticity gradient in a fluid is produced either by variation in the Coriolis parameter as a function of latitude or, for a homogeneous fluid, by variations in the bathymetry of the basin.

From an analytical point of view, the studies of free oscillations in enclosed water bodies of ideal shapes – such as circular, elliptic, or rectangular basins – for various simple depth variations have been considered by Rayleigh, Jeffreys, Lamb, Hidaka, and others (see Rao (1965) for a summary). These simple analytic shapes permit the treatment of the dynamical equations in their continuum form and sometimes provide simple closed solutions. However, when the Earth's rotation is considered, the mathematical problem of two dimensional free oscillations in an enclosed basin can become quite complicated even in the simple case of a rectangular basin of uniform depth (Rao 1965). The difficulty becomes even greater when a natural basin of some arbitrary shape and bathymetry is considered on a rotating Earth. The purpose of the present investigation is to develop a general method, which is capable of taking into account the shape, bathymetry and the Earth's rotation in determining the periods and structures of the normal modes in any enclosed basin.

In the context of oscillations in real lakes, several investigations were carried out by analysing water level records to determine the periods and structures of the free oscillations, most recent example of which is the very thorough analysis of Mortimer & Fee (1976) on Lake Superior and Lake Michigan. From investigations of this type, gravitational modes are readily identified in view of their shorter periods as compared to rotational modes. Consequently, the theoretical studies on free oscillations in enclosed natural basins have focused attention more on the gravitational modes than on the rotational modes. Most natural basins are narrow and elongated and the dominant oscillations correspond to the longitudinal modes of the basin. Classical formulation of the channel theory takes advantage of this longitudinal nature in simplifying the governing equations. In the channel theory, the Earth's rotation is ignored and the two dimensional problem

[†] Exceptions arise in enclosed basins. Depending upon the relative values of f, length of the basin and depth of the fluid, some gravitational modes may have frequencies $\sigma < f$ (see Rao 1965).

in the horizontal plane is reduced to a corresponding one dimensional (in the direction of the longitudinal axis) problem by introducing equations that are averaged in the transverse direction. Application of these channel equations to real lakes has proved very satisfactory for the determination of the periods of some of the lowest longitudinal modes in narrow lakes (Defant 1961).

The solutions of channel equations, even though satisfactory as far as values of oscillation periods are concerned, do not give structures of the modes that are in agreement with observed characteristics. The channel equations yield only standing wave solutions with nodal lines fixed in space for all time. Observations indicate that nodal lines tend to rotate around a basin with time and for the lowest longitudinal mode, this rotation of the nodal line – and the consequent propagation of high water – always is in the counterclockwise direction. Such a behaviour of the lowest mode may be simulated in the framework of the channel theory by the imposition of Kelvin wave dynamics on the solutions (see, for example, Defant 1953; Platzman & Rao 1964).

Even though the imposition of Kelvin wave dynamics on the channel solutions gives very satisfactory results for the lowest mode, its validity for the higher modes breaks down both quantitatively and qualitatively. Kelvin wave hypothesis leads to amphidromic systems, all of which propagate in the counterclockwise direction in the northern hemisphere. Observations of Mortimer & Fee (1976) and theoretical calculations of Rao (1965), for example, indicate that in an enclosed basin both positively (counterclockwise) and negatively (clockwise) propagating amphidromic systems are possible. Moreover, validity of the channel equations breaks down for basins like Lake Superior which are not narrow and elongated.

In addition to the gravitational modes, a basin with variable bottom topography on a rotating plane also exhibits a spectrum of rotational modes as mentioned earlier. In the above described channel theory, these rotational modes are of course completely suppressed. Even though it is difficult to resolve the properties of rotational modes in natural basins from water level data, these modes are nonetheless present in the system and their role would be important in the long period behaviour of a lake.

From the preceding discussion it is clear that a satisfactory treatment of the free oscillations in an arbitrary basin requires an attack on the full two dimensional problem. Loomis (1973) has considered the two dimensional problem in irregular basins in the absence of rotation. Platzman (1972) treated the two dimensional problem with rotation by the use of resonance iteration method and determined the period and structure of the lowest mode in Lakes Erie and Superior as well as the Gulf of Mexico. However, application of this procedure to higher modes becomes rather complicated.† Hamblin (1972) used an inverse iteration procedure to obtain some of the lowest gravitational modes and a rotational mode in Lake Ontario.

Proudman (1916) developed an elegant analytical procedure for determining the two dimensional free oscillations of a water body. This theory has been used by Rao (1965) and more recently by Longuet-Higgins & Pond (1970) in studying the free oscillation problems in ideal cases. In the present work, Proudman's method has been used in the discretized form to determine the normal modes of arbitrary basins. The frequencies and structures of the modes are computed as the eigenvalues and eigenvectors associated with a Hermitian matrix. The procedure yields several of the lowest gravitational modes and several rotational modes.

† Since then, Platzman (1975) applied a more efficient method (due to Lanczos) to determine several normal modes of the combined Atlantic–Indian Ocean system.

2. Governing equations

We are concerned with the quasi-static (or shallow water) dynamics of an incompressible homogeneous fluid on a rotating Cartesian plane. Let $f(\equiv 2\omega\sin\theta)$ be the local Coriolis parameter where ω is the angular speed of rotation of the Earth and θ is the latitude. $\boldsymbol{V}$ ($\equiv u, v$) is the horizontal velocity vector with components u in the x-direction (towards east) and v in the y-direction (towards north). The depth of the fluid in equilibrium is $H = H(x, y)$ and η is the departure of the water level from the mean. Letting g denote the apparent gravitational force per unit mass the linearized shallow water equations can be written in terms of the transport-vector $H\boldsymbol{V} \equiv \boldsymbol{M}$ ($\equiv M, N$) as

$$
\left.
\begin{aligned}
\frac{\partial \boldsymbol{M}}{\partial t} - f[\boldsymbol{M}] &= -g\bar{H}h\nabla\eta, \\
\frac{\partial \eta}{\partial t} + \nabla\cdot\boldsymbol{M} &= 0.
\end{aligned}
\right\}
\tag{2.1}
$$

In the above equations, ∇ is the horizontal gradient operator and [ ] denotes a rotation of the vector through a right angle in the clockwise direction of the horizontal plane. $h(x, y) \equiv H(xy)/\bar{H}$ is a proxy for dimensional depth H. $\bar{H}$ is some constant depth. For an enclosed basin, the appropriate boundary conditions to be adjoined to equations (2.1) are simply the adiabatic boundary conditions,

$$
\boldsymbol{M}\cdot\boldsymbol{n} = h\boldsymbol{V}\cdot\boldsymbol{n} = 0
\tag{2.2}
$$

on the coast. $\boldsymbol{n}$ is the outward drawn normal to the coast line. Equations (2.1), (2.2) completely specify the problem and one has to seek harmonic solutions in time of the form $e^{i\sigma t}$, where σ is the frequency of oscillation, to solve for the normal mode problem. Perhaps a simple approach would be to eliminate two of the dependent variables (say the transport components M, N) in terms of the third one η. Such an elimination results in a single equation

$$
\nabla\cdot h\nabla\eta + \left(\frac{\sigma^2 - f^2}{g\bar{H}}\right)\eta + \frac{if}{\sigma}\nabla h\cdot[\nabla\eta] = 0.
\tag{2.3}
$$

The boundary conditions (2.2) in terms of η become

$$
\frac{\partial \eta}{\partial n} - \frac{if}{\sigma}\frac{\partial \eta}{\partial s} = 0
\tag{2.4}
$$

on the coast. n and s are the normal and tangential derivatives to the coast.

The reduction of equations (2.1) into one equation (2.3) may be convenient since the characteristic value problem (2.3, 4) involves a second order elliptic differential operator (the tidal operator) and only one scalar dependent variable. However, the disadvantage introduced by such a formulation is that the problem now becomes an 'irregular' eigenvalue problem both due to the fact that σ appears in the tidal operator as well as in the boundary conditions. For this reason, in the method used here, we directly attack the equations in their 'primitive' form as described in the next section.

3. Analytical basis for the method of solution

The procedure followed here is one that was developed originally by Proudman (1916) from a Lagrangian point of view and discussed from an Eulerian point of view by Rao (1965). This method has so far been only applied to the cases of ideal geometry, the most recent study along

these lines being that of Longuet-Higgins & Pond (1970). However, Proudman's method can also be applied to natural basins through the use of finite differences in space. We first present below a brief outline of the analytical theory for obtaining the solution and then the numerical method.

The transport vector M is independent of depth and may be partitioned into two parts M^ϕ and M^ψ such that

$$M \equiv M^\phi + M^\psi, \tag{3.1}$$

where M^ϕ and M^ψ are given in terms of two scalar functions ϕ and ψ:

$$M^\phi \equiv -h\nabla\phi, \quad M^\psi \equiv -[\nabla\psi]. \tag{3.2}$$

ϕ and ψ are the potential and stream function for the transport field. It is seen from equation (3.2) that M^ψ is the solenoidal part of M and $h^{-1}M^\phi$ is the irrotational part. That is,

$$\nabla\cdot[h^{-1}M^\phi] = 0 \quad \text{and} \quad \nabla\cdot M^\psi = 0. \tag{3.3}$$

The boundary condition $M\cdot n = 0$ is satisfied by adjoining the conditions

$$M^\phi\cdot n = 0, \quad M^\psi\cdot n = 0. \tag{3.4}$$

In terms of ϕ and ψ, the preceding condition becomes

$$h\frac{\partial\phi}{\partial n} = 0, \quad \psi = 0 \tag{3.5}$$

on the boundary.

The procedure for determining M now proceeds by examining the divergence of the mass field and vorticity of the velocity field. These are given by

$$\left.\begin{aligned} \nabla\cdot h\nabla\phi &= -\nabla\cdot M, \\ \nabla\cdot h^{-1}\nabla\psi &= \nabla\cdot[h^{-1}M]. \end{aligned}\right\} \tag{3.6}$$

If M is prescribed as a function of the horizontal coordinates the right sides of (3.6) are known and each of these equations represents an inhomogeneous elliptic partial differential equation with homogeneous boundary condition (3.5). It is well known that such a problem has unique solution.

However, since M itself is an unknown, but satisfies the dynamical equations, the procedure now is to convert the governing equations into conditions on ϕ and ψ in terms of orthogonal-function expansions. A natural choice for these orthogonal functions will be the set of characteristic functions associated with the differential operators

$$L_1 \equiv \nabla\cdot h\nabla \quad \text{and} \quad L_2 \equiv \nabla\cdot h^{-1}\nabla$$

that appear in equation (3.6).

Let λ_α and $\phi_\alpha(x,y)$ be the characteristic values and characteristic functions associated with the operator L_1; that is,

$$L_1\phi_\alpha = -\lambda_\alpha\phi_\alpha, \quad h\frac{\partial\phi\alpha}{\partial n} = 0 \quad \text{on the boundary.} \tag{3.7a}$$

Similarly, let μ_α and ψ_α be the characteristic values and functions of L_2 so that

$$L_2\psi_\alpha = -\mu_\alpha\psi_\alpha, \quad h^{-1}\psi_\alpha = 0 \quad \text{on the boundary.}† \tag{3.7b}$$

† $h^{-1}\psi_\alpha = 0$ on the boundary imposes a stronger condition than required by (3.5). However, it is necessary to make (3.7b) self-adjoint.

In $(3.7\,a, b)$, α is a binary index used for enumeration of the characteristic functions (also referred to as spectral functions). It is clear that the problems $(3.7\,a, b)$ are self-adjoint. Hence, the characteristic values λ_α, μ_α are real and the associated functions ϕ_α and ψ_α each form a complete and internally orthogonal set. Without loss of any generality, the orthogonality condition may be chosen as

$$\left.\begin{array}{l} \int h^{-1} \boldsymbol{M}_\alpha^\phi \cdot \boldsymbol{M}_\beta^\phi \, \mathrm{d}A = \lambda_\alpha \int \phi_\alpha \phi_\beta \, \mathrm{d}A = Ac^2 \bar{H}^2 \delta_{\alpha\beta}, \\[2mm] \int h^{-1} \boldsymbol{M}_\alpha^\psi \cdot \boldsymbol{M}_\beta^\psi \, \mathrm{d}A = \mu_\alpha \int \psi_\alpha \psi_\beta \, \mathrm{d}A = Ac^2 \bar{H}^2 \delta_{\alpha\beta}, \end{array}\right\} \tag{3.8}$$

where $c^2 \equiv g\bar{H}$ and A is the surface area of the basin.

$$\delta_{\alpha\beta} = \begin{cases} 1 & \text{if} \quad \alpha = \beta, \\ 0 & \text{if} \quad \alpha \neq \beta. \end{cases}$$

We have further defined, in accordance with (3.2),

$$\boldsymbol{M}_\alpha^\phi \equiv -h\nabla\phi_\alpha, \quad \boldsymbol{M}_\alpha^\psi = -[\nabla\psi_\alpha] \tag{3.9}$$

in the orthogonality condition (3.8).

Define now the (non-dimensional) expansion coefficients

$$\left.\begin{array}{l} P_\alpha \equiv \dfrac{1}{c^2 A \bar{H}^2} \int h^{-1} \boldsymbol{M}_\alpha^\phi \cdot \boldsymbol{M}^\phi \, \mathrm{d}A = \dfrac{1}{c^2 A \bar{H}^2} \int h^{-1} \boldsymbol{M}_\alpha^\phi \cdot \boldsymbol{M} \, \mathrm{d}A, \\[3mm] Q_\alpha \equiv \dfrac{1}{c^2 A \bar{H}^2} \int h^{-1} \boldsymbol{M}_\alpha^\psi \cdot \boldsymbol{M}^\psi \, \mathrm{d}A = \dfrac{1}{c^2 A \bar{H}^2} \int h^{-1} \boldsymbol{M}_\alpha^\psi \cdot \boldsymbol{M} \, \mathrm{d}A \end{array}\right\} \tag{3.10}$$

to represent $\boldsymbol{M}^\phi$ and $\boldsymbol{M}^\psi$. In view of the orthogonality condition (3.8), the sums on the right of

$$\left.\begin{array}{l} \boldsymbol{M}^\phi = \sum\limits_\alpha P_\alpha \boldsymbol{M}_\alpha^\phi, \\[2mm] \boldsymbol{M}^\psi = \sum\limits_\alpha Q_\alpha \boldsymbol{M}_\alpha^\psi, \end{array}\right\} \tag{3.11}$$

are the least squares approximations to $\boldsymbol{M}^\phi$ and $\boldsymbol{M}^\psi$ when the sums span the complete spectra of (3.7).

So far the orthogonal bases are established only for $\boldsymbol{M}^\phi$ and $\boldsymbol{M}^\psi$. It still remains to establish a set of basis functions for the representation of the height field η. An examination of the continuity equation reveals that η is governed by the divergent part of $\boldsymbol{M}$. Hence, ϕ_α form a sufficient basis for η. For convenience, define

$$\eta_\alpha \equiv c^{-1}(\lambda_\alpha)^{\frac{1}{2}} \phi_\alpha. \tag{3.12}$$

The orthonormality relation among the η_α's may be stated as

$$\int \eta_\alpha \eta_\beta \, \mathrm{d}A = A\bar{H}^2 \delta_{\alpha\beta}. \tag{3.13}$$

If R_α are the expansion coefficients for the η-field, then

$$\eta = \sum_\alpha R_\alpha \eta_\alpha, \tag{3.14}$$

where

$$R_\alpha = \frac{1}{A\bar{H}^2} \int \eta_\alpha \eta \, \mathrm{d}A. \tag{3.15}$$

Expressions (3.11) and (3.14) now formally complete the representation of the dependent variables of the problem.

Substitution of the expansions (3.11, 14) into the dynamical equations (2.1) and isolation of the expansion coefficients by the usual procedure results in the following system of prediction equations:

$$\left.\begin{aligned}\frac{dP_\alpha}{dt} - \sum_\beta A_{\alpha\beta} P_\beta - \sum_\beta B_{\alpha\beta} Q_\beta - \nu_\alpha R_\alpha &= 0, \\ \frac{dQ_\alpha}{dt} - \sum_\beta C_{\alpha\beta} P_\beta - \sum_\beta D_{\alpha\beta} Q_\beta &= 0, \\ \frac{dR_\alpha}{dt} + \nu_\alpha P_\alpha &= 0. \end{aligned}\right\} \tag{3.16}$$

In the preceding equations, the following definitions have been introduced:

$$\left.\begin{aligned} A_{\alpha\beta} &\equiv \{M_\alpha^\phi, [M_\beta^\phi]\}, & B_{\alpha\beta} &\equiv \{M_\alpha^\phi, [M_\beta^\psi]\}, \\ C_{\alpha\beta} &\equiv \{M_\alpha^\psi, [M_\beta^\phi]\}, & D_{\alpha\beta} &\equiv \{M_\alpha^\psi, [M_\beta^\psi]\}, \end{aligned}\right\} \tag{3.17}$$

where the notation $\{A, B\}$ represents an inner product of two vectors according to

$$\{A, B\} \equiv \frac{1}{c^2 A \bar{H}^2} \int f h^{-1} A \cdot B \, dA.$$

The coefficients $A_{\alpha\beta}$, etc. are numerical constants which include the effect of a variable Coriolis parameter and the effect of topography. These coefficients also may be seen to have the following properties

$$\left.\begin{aligned} A_{\alpha\beta} &= -A_{\beta\alpha}, \\ B_{\alpha\beta} &= -C_{\beta\alpha}, \\ D_{\alpha\beta} &= -D_{\beta\alpha}. \end{aligned}\right\} \tag{3.18}$$

The parameter ν_α in equations (3.16) represents

$$\nu_\alpha \equiv (c^2 \lambda_\alpha)^{\frac{1}{2}}. \tag{3.19}$$

When $f = 0$, it is seen from (3.17) that all the coefficients $A_{\alpha\beta}$, etc. are equal to zero. The system of equations (3.16) then simply reduce to an equation of the type

$$d^2 P_\alpha / dt^2 = -\nu_\alpha^2 P_\alpha,$$

which shows that ν_α is the frequency of oscillations in the non-rotating case.

In working towards a solution of the spectral–dynamical equations (3.16), it is necessary to order the wavenumber vector index α with respect to a single scalar index. The specific manner in which this ordering is arranged is rather arbitrary and will be explained later. For the present, it suffices to assume such an ordering can be done and let it be designated by scalar indices $i = 1, 2, 3, \ldots$ or $j = 1, 2, 3, \ldots$. For convenience, then, we denote

$$P_i \equiv P_{\alpha i}, \quad Q_i \equiv Q_{\alpha i}, \quad R_i \equiv R_{\alpha i}, \quad \nu_i \equiv \nu_{\alpha i}.$$

Define now column vectors

$$\left.\begin{aligned} \bar{P} &\equiv \mathrm{col}\,(P_i), \quad \bar{Q} \equiv \mathrm{col}\,(Q_i), \quad \bar{R} \equiv \mathrm{col}\,(R_i), \\ \bar{s} &\equiv \begin{pmatrix} \bar{P} \\ \bar{Q} \\ \bar{R} \end{pmatrix} \end{aligned}\right\} \tag{3.20}$$

and matrices

$$A \equiv |A_{ij}|, \quad B \equiv |B_{ij}|, \atop C \equiv |C_{ij}|, \quad D \equiv |D_{ij}|, \biggr\} \tag{3.21}$$

$$\langle \nu \rangle \equiv \text{diagonal } \nu_i.$$

Equations (3.16) may now be written in the following form:

$$\mathrm{d}\bar{s}/\mathrm{d}t + a\bar{s} = 0, \tag{3.22}$$

where a is a square matrix

$$a \equiv \begin{bmatrix} -A & -B & -\langle\nu\rangle \\ -C & -D & 0 \\ \langle\nu\rangle & 0 & 0 \end{bmatrix}. \tag{3.23}$$

In (3.22), if we now assume that

$$\bar{s} \sim \mathrm{e}^{\mathrm{i}\sigma t},$$

where σ is the frequency of oscillation, equation (3.22) becomes

$$\mathrm{i}\sigma\bar{s} + a\bar{s} = 0 \quad \text{or} \quad (\sigma I - \mathrm{i}a)\,\bar{s} = 0, \tag{3.24}$$

where I is the identity matrix. Equation (3.24) shows that σ's are the characteristic values of the matrix $\mathrm{i}a$. From (3.21) and (3.23), it is clear that the matrix $\mathrm{i}a$ has Hermitian symmetry. Hence, the characteristic values σ are real.

The characteristic values σ of the matrix (3.24) simply represent the frequencies of free oscillation of the basin under consideration. These frequencies will have to be determined by a numerical procedure after choosing some appropriate size for truncation of the matrix. Once the frequencies are obtained (by some numerical eigenvalue algorithm), the associated eigenvectors $\bar{s}$ can be calculated. Using expansions (3.11) and (3.14), then, one can construct the structure of the various normal modes. As mentioned earlier, these normal modes fall into two distinct categories: the inertia-gravitational and the rotational modes (modified by divergence). If the secular determinant is truncated at a size $n \times n$ (say), then we obtain $\frac{2}{3}n$ gravitational modes and $\frac{1}{3}n$ rotational modes, in pairs (plus and minus the same value). If the basin has a uniform depth and Coriolis parameter is constant the modes of the latter class become evanescent.

The discussion so far only dealt with the formal framework of setting up the characteristic value problem for an arbitrary basin. The essence of the problem depends upon solving for the orthogonal set of basis functions as defined by the homogeneous elliptic self-adjoint problems (3.7 a,b). For an arbitrary basin, one has to resort to numerical methods to construct these orthogonal functions. This aspect of the problem is discussed in the next section.

4. NUMERICAL CONSTRUCTION OF THE BASIS FUNCTIONS

The basis functions are generated from the elliptic equations (3.7). These equations, together with the boundary conditions, define a self-adjoint problem in the continuum, that is,

$$\int \phi_\beta \nabla \cdot h\nabla\phi_\alpha \, \mathrm{d}A = \int \phi_\alpha \nabla \cdot h\nabla\phi_\beta \, \mathrm{d}A, \atop \int \psi_\beta \nabla \cdot h^{-1}\nabla\psi_\alpha \, \mathrm{d}A = \int \psi_\alpha \nabla \cdot h^{-1}\nabla\psi_\beta \, \mathrm{d}A, \biggr\} \tag{4.1}$$

where ϕ_β and ψ_β are two other functions obeying the same boundary conditions as ϕ_α and ψ_α respectively.

In the case of an arbitrary basin, where a solution is sought for (3.7) in the domain of a discretized (finite difference) system, care should be exercised in the formulation of the finite difference system. Otherwise, the self-adjoint property will be destroyed for the discrete system resulting in spurious complex values for λ_α (or μ_α). We choose here a grid for the ϕ_α and ψ_α problems as indicated in figure 1. The x and y coordinates are replaced by discrete points $x_j = j\Delta x/2$ and $y_k = k\Delta y/2$ where j and k are integers. The ϕ_α's and ψ_α's are defined at all points such that

$$j = \text{even}, \quad k = \text{even for } \phi_\alpha,$$

$$j = \text{odd}, \quad k = \text{odd for } \psi_\alpha.$$
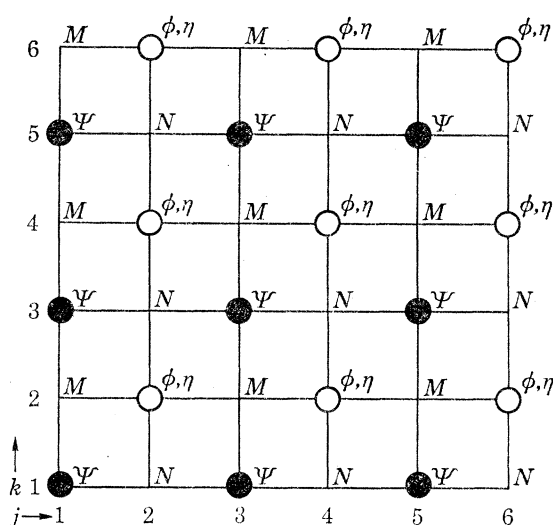
FIGURE 1. Distribution of variables on the numerical grid.

Since the basis functions η_α are proportional to ϕ_α they are also defined at the same points as ϕ_α's. This type of a choice for ϕ_α, ψ_α, and η_α results in a dispersion of the dependent variables M, N, and η as indicated on the figure 1 representing what is known as a single Richardson lattice. The boundary of the basin passes through only the ψ_α-points.

Equations (3.7) are now written in a finite difference form on the grid of figure 1 in the following form (suppressing the binary index α).

For all j even, k even

$$\frac{(h\,\partial\phi/\partial x)_{j+1,k} - (h\,\partial\phi/\partial x)_{j-1,k}}{\Delta x} + \frac{(h\,\partial\phi/\partial y)_{j,k+1} - (h\,\partial\phi/\partial y)_{j,k-1}}{\Delta y} = -\lambda\phi_{j,k}. \tag{4.2}$$

The first order derivatives in (4.2) are further replaced by central differences yielding

$$\frac{h_{j+1,k}(\phi_{j+2,k} - \phi_{j,k})}{\Delta x^2} - \frac{h_{j-1,k}(\phi_{j,k} - \phi_{j-2,k})}{\Delta x^2} + \frac{h_{j,k+1}(\phi_{j,k+2} - \phi_{j,k})}{\Delta y^2} - \frac{h_{j,k-1}(\phi_{j,k} - \phi_{j,k-2})}{\Delta y^2} = -\lambda\phi_{j,k}. \tag{4.3}$$

for all interior points. If a point $j \pm 1$, k falls on a boundary perpendicular to x-direction then the appropriate $(h\,\partial\phi_\alpha/\partial x)$ is set equal to zero and if a point $j, k \pm 1$ falls on a boundary normal to

y-direction, the appropriate $(h\, \partial\phi_\alpha/\partial y)$ is set equal to zero according to the boundary condition (3.7 a). Solution of the preceding problem alone will give the two dimensional non-rotating oscillation frequencies and structures, and corresponds essentially to the work of Loomis (1973).

For all j odd, k odd

$$\frac{(h^{-1}\,\partial\psi/\partial x)_{j+1,\,k} - (h^{-1}\,\partial\psi/\partial x)_{j-1,\,k}}{\Delta x} + \frac{(h^{-1}\,\partial\psi/\partial y)_{j,\,k+1} - (h^{-1}\,\partial\psi/\partial y)_{j,\,k-1}}{\Delta y} = -\mu\psi_{j,\,k}. \qquad (4.4)$$

On further expressing the first order derivatives by central differences, we obtain

$$\frac{h^{-1}_{j+1,\,k}(\psi_{j+2,\,k} - \psi_{j,\,k})}{\Delta x^2} - \frac{h^{-1}_{j-1,\,k}(\psi_{j,\,k} - \psi_{j-2,\,k})}{\Delta x^2}$$

$$+ \frac{h^{-1}_{j,\,k+1}(\psi_{j,\,k+2} - \psi_{j,\,k})}{\Delta y^2} - \frac{h^{-1}_{j,\,k-1}(\psi_{j,\,k} - \psi_{j,\,k-2})}{\Delta y^2} = -\mu\psi_{j,\,k}. \qquad (4.5)$$

In (4.5), if a point $j \pm 2, k$ or $j, k \pm 2$ falls on a boundary the corresponding ψ is set equal to zero (in accordance with 3.7 b).

When the continuum equations (3.7) are transformed into the discrete domain according to the above described procedure, it is possible to show that the self-adjoint property remains valid for the discrete set of equations (4.3) and (4.5). That is

$$\sum_{j,\,k} \phi'_{j,\,k}(\nabla \cdot h\nabla\phi)_{j,\,k} = \sum_{j,\,k} \phi_{j,\,k}\nabla \cdot h\nabla\phi'_{j\,k},$$

$$\sum_{j,\,k} \psi'_{j,\,k}(\nabla \cdot h^{-1}\nabla\psi)_{j,\,k} = \sum_{j,\,k} \psi_{j,\,k}\nabla \cdot h^{-1}\nabla\psi'_{j,\,k},$$

where the indices j, k span all the ϕ-points or the ψ-points, depending on the equation being considered. ϕ' and ψ' are two other functions obeying the same boundary condition as ϕ and ψ.

When the equations (4.3) or (4.5) are written out explicitly for any arbitrary water body, the elements $(\phi)_{j,\,k}$ or $(\psi)_{j,\,k}$ can be ordered as a one dimensional column vector and the set of simultaneous equations may be written in a matrix form

$$\boldsymbol{G}\overline{\phi} = -\lambda\overline{\phi}, \quad \boldsymbol{H}\overline{\psi} = -\mu\overline{\psi}. \qquad (4.6)$$

The coefficients of matrixes $\boldsymbol{G}$ and $\boldsymbol{H}$ are obtained from (4.3) and (4.5) respectively. From (4.6), it is seen that λ and μ are the characteristic values of $\boldsymbol{G}$ and $\boldsymbol{H}$ and may be determined by the use of standard eigenvalue procedures. The various λ's and μ's and associated ϕ's and ψ's then represent the various λ_α's and μ_α's and ϕ_α's and ψ_α's necessary for the procedure described in § 3.

In forming the coupling coefficients, the wave number vector α has to be ordered with respect to a scalar index i as mentioned earlier. This has been done in the following manner. Since the primary interest will be focused on those modes with the largest space scales, and the characteristic values λ_α and μ_α have the nature of (wavenumber)^2, retaining the lowest values of λ_α and μ_α at any order of truncation of the final matrix will result in the inclusion of all the largest space scales up to that point. On this basis, the scalar ordering for α is done such that λ_i and μ_i form an ascending sequence of numbers: $\lambda_1 < \lambda_2 < \lambda_3 \ldots$ and $\mu_1 < \mu_2 < \mu_3 \ldots$. The coupling coefficients Aij, etc. are then obtained by the following procedure

$$Aij = \frac{f}{c^2 A \overline{H}^2} \int h^{-1} \boldsymbol{M}^\phi_i \cdot [\boldsymbol{M}^\phi_j]\, \mathrm{d}A$$

$$= f\frac{\Delta x \Delta y}{c^2 A \overline{H}^2} \sum_{\phi\text{-points}} (h^{-\frac{1}{2}}M^\phi_i)(h^{-\frac{1}{2}}N^\phi_j) - (h^{-\frac{1}{2}}N^\phi_i)(h^{-\frac{1}{2}}M^\phi_j). \qquad (4.7)$$

Where, for example,

$$-h^{-\frac{1}{2}}M_i^\phi \equiv h^{\frac{1}{2}}\left(\frac{\partial\phi_i}{\partial x}\right) = \frac{1}{2}\left\{\left(h^{\frac{1}{2}}\frac{\partial\phi_i}{\partial x}\right)_{j+1,k} + \left(h^{\frac{1}{2}}\frac{\partial\phi_i}{\partial x}\right)_{j-1,k}\right\}$$

$$= \frac{1}{2\Delta x}\{h_{j+1,k}^{\frac{1}{2}}[(\phi_i)_{j+2,k} - (\phi_i)_{j,k}] + h_{j-1,k}^{\frac{1}{2}}[(\phi_i)_{j,k} - (\phi_i)_{j-2,k}]\}.$$

Similarly, the other terms in (4.7) are obtained as well as the other coupling coefficients Bij, ($Cij = -Bji$) and Dij. The formula in (4.7) is written as if the Coriolis parameter f is a constant. It is, however, clear that if f were to be considered a variable parameter, it is a straightforward matter to incorporate that variation into formula (4.7). After all the necessary coefficients Aij, etc., are calculated, the coefficient matrix (3.23) is formulated and once again solved as an ordinary eigenvalue problem.

5. Test of the numerical algorithm

The numerical algorithm described in the preceding section has been tested against some simple cases for which results are available from purely analytic or quasi-analytic considerations. The first test was carried out for the case of a rectangular basin of uniform depth. The characteristic value problems (3.7 a, b) may then be solved exactly. The solutions are (with $h = 1$ for uniform depth):

$$\phi_\alpha = \hat{\phi}_\alpha \cos\frac{k\pi x}{a}\cos\frac{l\pi y}{b} \quad (k = 0, 1, 2, \dots; l = 0, 1, 2, \dots),$$

$$\psi_\alpha = \hat{\psi}_\alpha \sin\frac{k\pi x}{a}\sin\frac{l\pi y}{b} \quad (k = 1, 2, 3, \dots; l = 1, 2, 3, \dots),$$

$$\lambda_\alpha = \frac{\pi^2}{a^2}\left(k^2 + \frac{a^2}{b^2}l^2\right) = \mu_\alpha. \tag{5.1}$$

Here (k, l) are the scalar components of the vector α. The amplitudes $\hat{\phi}_\alpha$, $\hat{\psi}_\alpha$ are defined so as to satisfy the orthonormality conditions (3.8), a and b are the length and breadth of the basin. b/a is taken as $1.01/1$ to avoid degeneracies in the spectrum of eigenvalues. The characteristic values from the numerical formulation (equation 4.6) are compared in table 1 with the exact analytic values from equation (5.1). The various modes of velocity potential and stream function are identified by the number of nodal lines in the x and y directions. For the potential field, the number of nodal lines in each direction are given by the values of k and l and for the stream function by $(k-1)$ and $(l-1)$. In calculating the results of table 1, 10 intervals are chosen in each direction ($\Delta x = \frac{1}{10}a$, $\Delta y = \frac{1}{10}b$) to transform the continuous equations into the discrete domain. An examination of table 1 shows an excellent agreement between the exact analytic results and the numerically determined ones.

The next test was performed on a rotating rectangular basin of uniform depth for which results are available from a quasi-analytic treatment by Rao (1965). The value of the Coriolis parameter was chosen such that $f/\nu_1 = 1.0$, where ν_1 corresponds to the lowest gravitational mode frequency in the no-rotational case. From the preceding calculation presented in table 1, the numerically determined functions ϕ_i and ψ_i corresponding to the lowest thirty λ_i's and thirty μ_i's are included in forming the coefficient matrix (3.23). The aspect ratio of the rectangular basin is chosen as 1.01×1 and the results are compared in table 2, to those corresponding to a square basin of Rao (1965). (It is reasonable to assume that a 1 % perturbation of one of the sides of the basin will not

cause any significant changes in the frequency values.) The modes are identified here, by a comparison of their structures. Once again it is clear that the frequencies obtained from a complete numerical treatment of the problem agree very well with those obtained from a quasi-analytic approach.

TABLE 1. COMPARISON OF ANALYTIC AND NUMERICAL RESULTS FOR THE CHARACTERISTIC VALUES $\lambda_i^{\frac{1}{2}}$ AND $\mu_i^{\frac{1}{2}}$ IN THE CASE OF A RECTANGULAR BASIN OF UNIFORM DEPTH

k, l	velocity potential		stream function	
	numerical	analytic	numerical	analytic
0, 1	3.098	3.110	—	—
1, 0	3.129	3.142	—	—
1, 1	4.403	4.421	4.403	4.421
0, 2	6.119	6.221	—	—
2, 0	6.180	6.283	—	—
1, 2	6.873	6.969	6.873	6.969
2, 1	6.913	7.011	6.913	7.011
2, 2	8.697	8.842	8.697	8.842

TABLE 2. FREQUENCIES σ/ν_1 FOR AN ALMOST SQUARE BASIN (1.01×1) OF UNIFORM DEPTH FROM THE PRESENT NUMERICAL METHOD AND FOR A SQUARE BASIN OF UNIFORM DEPTH FROM RAO (1965): ROTATION RATE IN BOTH CASES IS $f/\nu_1 = 1.0$

mode	present method	Rao (1965)
(1, 0)	0.723	0.723
(1, 1)	1.309	1.313
(0, 1)	1.513	1.509
(1, 2)	2.046	2.058
(2, 0)	2.112	2.131
(0, 2)	2.289	2.293

TABLE 3. COMPARISON OF ROTATIONAL MODE FREQUENCIES IN A SQUARE BASIN

mode	analytic	numerical
(1, 1)	0.7071	0.7071
(1, 2)	0.4472	0.4472
(2, 1)	0.3162	0.3162

The final test performed on the programme is a comparison of the numerical results with analytic results for non-divergent rotational modes in a square basin. For simplicity, the rotational modes in the square basin are taken as those corresponding to a basin on a β-plane; that is, a plane on which the Coriolis parameter is allowed to vary linearly with y, the north–south coordinate, so that $\mathrm{d}f/\mathrm{d}y$ is a constant. The analytical formula for the frequency of the non-divergent rotational modes may be shown to be given by

$$\frac{\sigma}{a(\mathrm{d}f/\mathrm{d}y)} = \frac{1}{2\pi(m^2 + (a^2/b^2)\,n^2)^{\frac{1}{2}}} \quad (m = 1, 2, 3, \ldots; \; n = 1, 2, 3, \ldots), \qquad (5.2)$$

where a is the length of the basin in the x-direction. In the present method of calculation, the non-divergent assumption can be introduced by simply suppressing all the ϕ_i spectrum, which makes the coefficients A_{ij}, B_{ij}, and C_{ij} equal to zero. Such an artifice, of course, eliminates all the gravitational modes and corresponds to the classical quasi-geostrophic approximation which

is possible only in the framework of a vorticity formulation. Here, however, we are explicitly dealing with the primitive equation system. Numerical results obtained this way (with 10 ψ_i functions retained) are compared to those corresponding to (5.2) in table 3. These show very good agreement between the numerical and analytic procedures.

6. APPLICATION TO LAKES ONTARIO AND SUPERIOR

We consider now the application of the numerical procedure to two natural basins: one is Lake Ontario and the other Lake Superior. In both these cases, one dimensional (and non-rotating) channel calculations have previously been made by Rockwell (1966). Lake Ontario, being a narrow elongated basin, may be more suitable for a channel approximation than Lake Superior, which is a fairly wide basin. Even though one might expect a reasonable approximation to the period values of the longitudinal modes by the use of channel theory, the structures of the various modes will be affected by two dimensional effects in both lakes, as well as the effect of rotation. Furthermore, the spectrum of rotational modes can only be obtained when the complete two dimensional rotating problem is considered. The results for Lakes Ontario and Superior are presented below.

(a) Gravitational modes

We will first consider the case of gravitational modes in Lakes Ontario and Superior.

(i) Lake Ontario

Bathymetric data for Lake Ontario are obtained from chart no. 2 of the U.S. Lake Survey. A grid of 10.08 km between two successive ϕ-points or ψ-points is used as shown in figure 2. This gives a total of 177 points for the velocity potential field and 137 points for the stream function field.
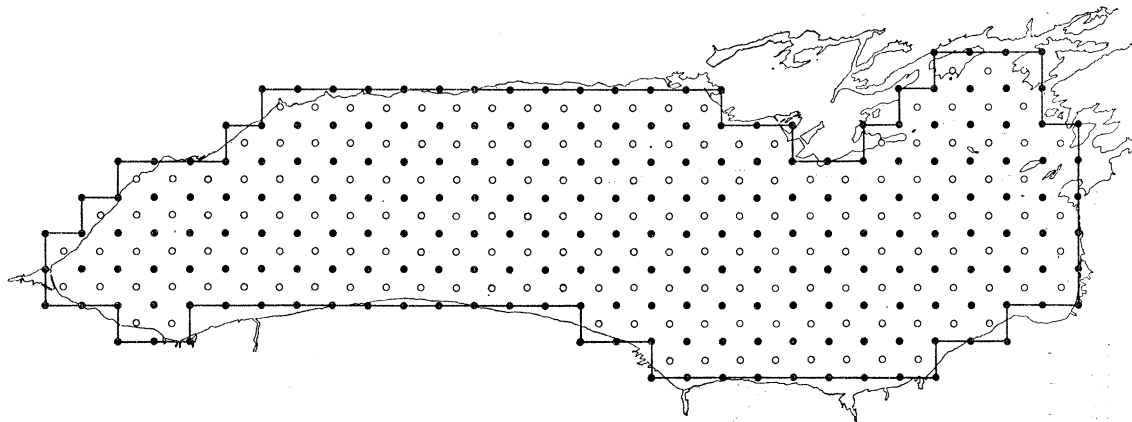

FIGURE 2. Numerical grid on Lake Ontario.

Although solutions for both of the basis functions ϕ_α and ψ_α have been numerically constructed, we will select some of the ϕ_α functions for examination since they represent the non-rotating, two dimensional modes of oscillation. Periods of some of the lowest modes of oscillation are given in table 4, along with those obtained from Rockwell's (1966) channel calculations. In the channel calculations, only the longitudinal modes are obtained whereas the two dimensional calculation can yield both longitudinal and transverse as well as a combination of both. However, the lowest

TABLE 4. COMPARISON OF NON-ROTATING PERIODS OF OSCILLATION FROM THE
TWO DIMENSIONAL THEORY AND CHANNEL THEORY

mode	period/h two dimensional result	channel result	percentage difference
1	5.10	4.91	3.9
2	3.11	2.97	4.7
3	2.31	2.15	7.4
4	1.87	—	—
5	1.78	1.63	9.2
6	1.45	1.29	12.4
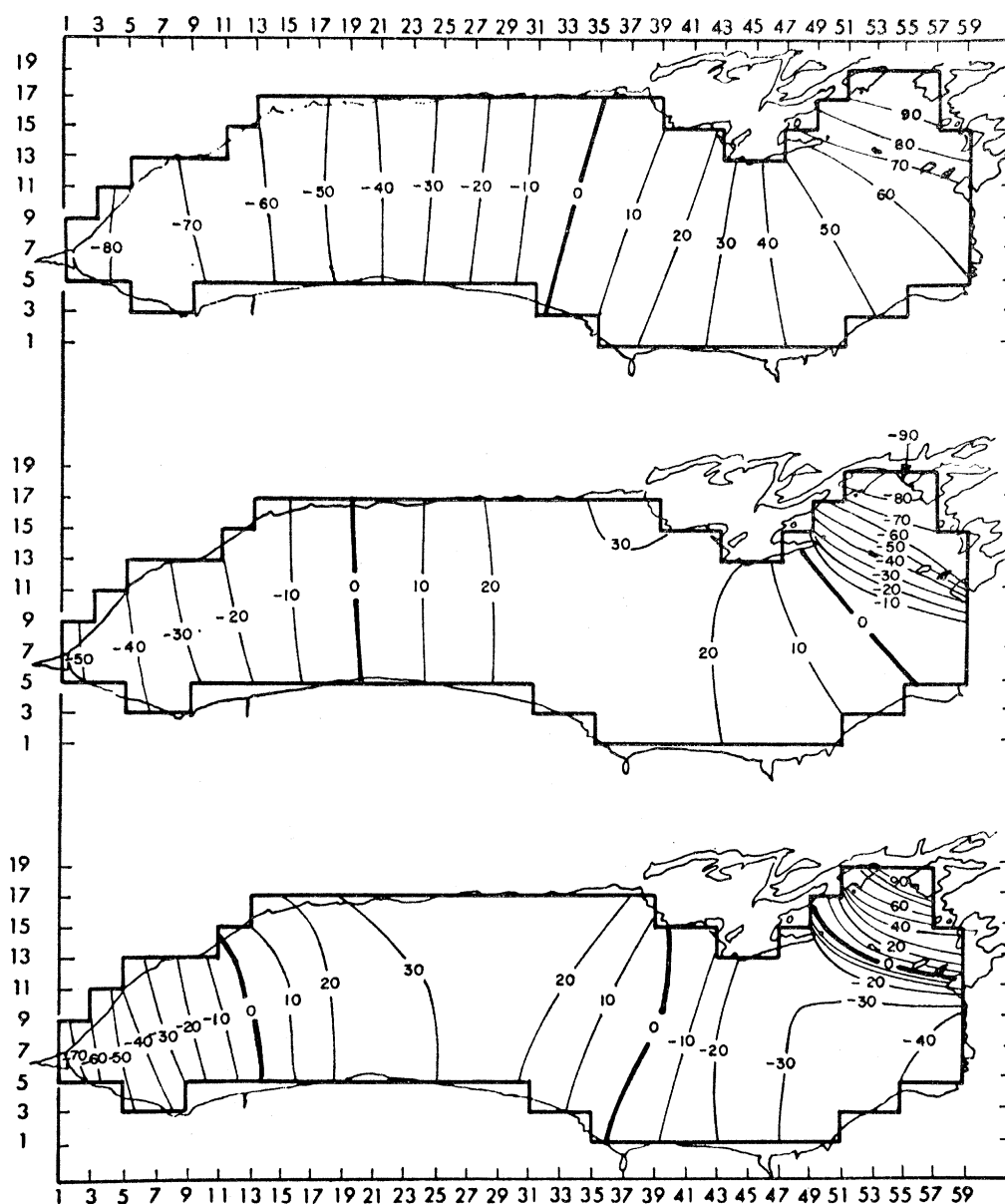
FIGURE 3. The first, second, and third non-rotating normal modes for Lake Ontario.

six modes in the present calculation seem to be of the longitudinal type. Some transverse oscillation effects appear from the seventh mode on.

Examination of the periods in table 4 indicates that two dimensional effect invariably appears to increase the period over the one dimensional channel calculation. The percentage increase in the periods increases with the modality as one might *a priori* anticipate since any basin will be less one dimensional the higher the modality of an oscillation. The two dimensional effect accounts for an increase of period of about 4 % for the fundamental mode and about 12 % for the fifth mode. The channel calculation periods are not available for modes higher than the fifth.

The structures of the lowest six modes are presented in figures 3 and 4 in terms of the height field η (which is similar to the potential field ϕ when rotation is zero). The modes here are of standing nature with nodal lines that are fixed in space for all time. In table 4, the fourth highest
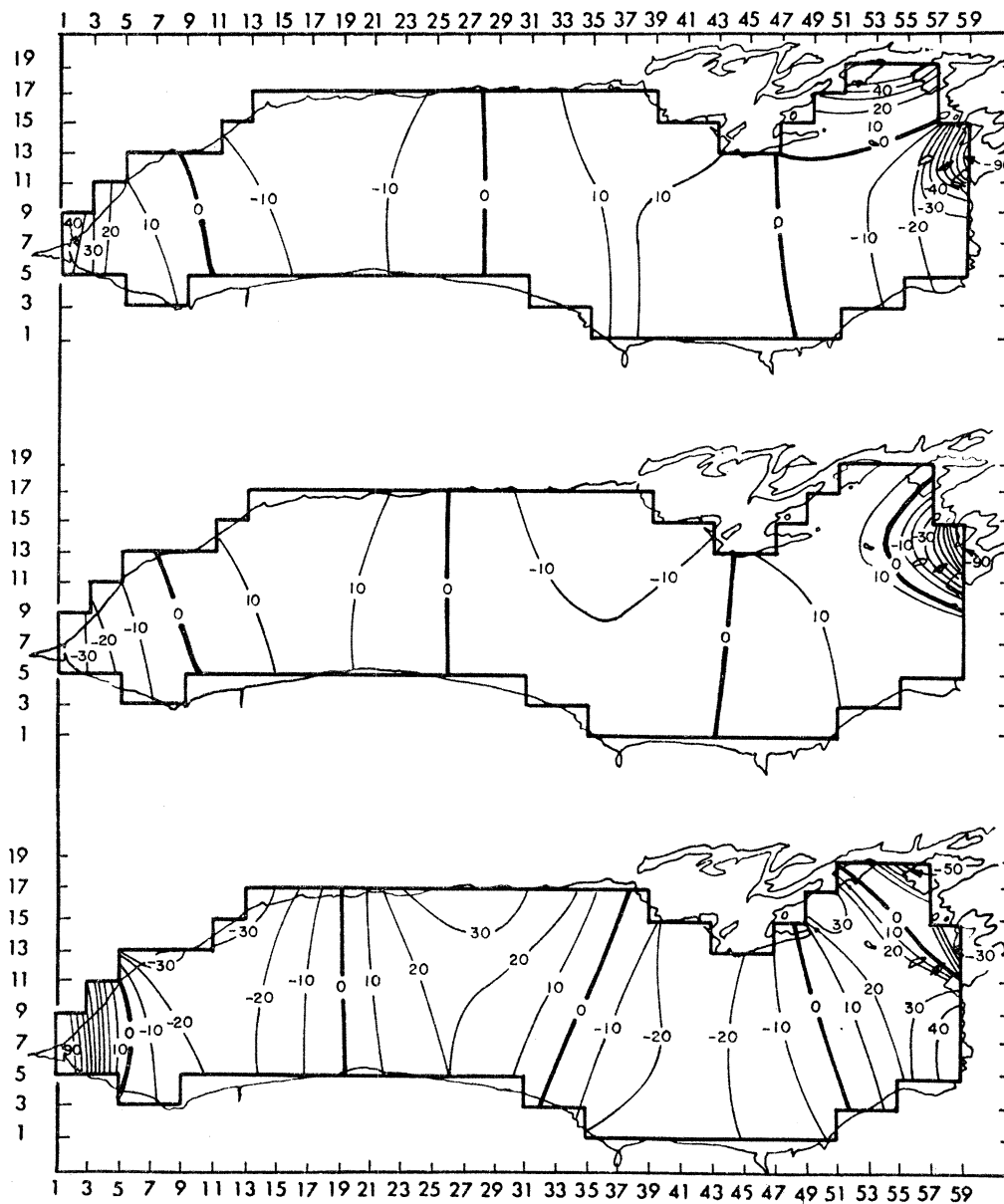
FIGURE 4. The fourth, fifth, and sixth non-rotating normal modes for Lake Ontario.

gravitational mode from the two dimensional calculation is 1.87 h. It is concluded by an examination of the structure of this mode, that it has been missed in the channel calculation of Rockwell. Hence, the fifth two dimensional mode has been tentatively designated as corresponding to the fourth mode from the channel calculation. In all of these diagrams, the amplitude of oscillation is so normalized that the highest value is 100 units.

The lowest mode has one nodal line oriented in a nearly N–S direction (note that the grid on Lake Ontario is rotated slightly from an x-east, y-north orientation for a better fit to the shape of the basin). The distribution of water level is nearly symmetric with respect to the nodal line with maximum values of η (or ϕ) on the boundary. The maximum water level fluctuation in the north-eastern shallows is larger than that in the western end and the gradient of water level along the channel axis is steeper in the north-eastern shallows. These same features are apparent in Rockwell's (1966) calculation of water level distribution along the channel axis.

The second mode has two nodal lines. The water level fluctuation is larger on the ends of the lake than in the area between the nodal lines with the largest fluctuation again in the north-eastern shallows. The gradient of water level along the channel axis is again very steep in the shallows. The third mode exhibits three nodal lines and a larger water level fluctuation on the ends of the basin than in the centre. Rockwell's (1966) one dimensional calculations show the same type of structure for the second and third modes.

The two dimensional effect is more clear from the structures of the fourth and fifth modes. Both of these modes have four nodal lines. The fourth mode appears to be a combination of a longitudinal oscillation coupled with a strong transverse oscillation which is primarily confined to the eastern end of the lake. The nodal line in the eastern end of the lake has a dominant east–west orientation. The fifth mode, which also has four nodal lines, appears to be more of a longitudinal fourth mode as one might expect from a channel consideration. The oscillation appears to be more dominant in the eastern end of the lake as compared to the rest of the lake. Finally, the sixth gravitational mode consists of five nodal lines and the structure of the mode appears like that of a fifth longitudinal mode.

TABLE 5. PERIODS OF THE LOWEST SIX GRAVITATIONAL MODES IN LAKE ONTARIO
WITH ROTATION

	period/h	
mode	present method	Hamblin's results
1	5.11	4.86
2	3.11	2.96
3	2.31	2.21
4	1.87	—
5	1.78	1.63
6	1.46	1.36

The normal modes of the lake with rotation are now built up by using several of the basis functions ϕ_α and ψ_α according to the procedure described in §§ 3 and 4. In the initial test the lowest 20 ϕ_α's and ψ_α's are included in formulating the matrix (3.23) and subsequently the lowest 50 and 80 ϕ_α's and ψ_α's are included. The difference in the periods of the lowest six gravitational modes between these truncations is very insignificant. In table 5, above, are presented the periods of the lowest six gravitational modes obtained from the matrix resulting from 80 vector truncation. Also given in the table are the period values obtained by Hamblin (1972.)

A comparison of these periods with those in table 4 indicates that rotation has negligible effect on the periods of these modes. This conclusion may be anticipated *a priori* in view of the elongated nature of the basin and the relatively small value of rotation speed in comparison with the slowest non-rotating gravitational mode frequency.

The structures of the lowest six gravitational modes are illustrated in figures 5 and 6 in terms of the fluctuation of free surface height. In these diagrams, solid lines indicate cotidal lines and the dashed lines represent co-range lines. These are calculated by writing the solution for the η field as

$$\eta = \mathrm{Re} \sum_\alpha R_\alpha \eta_\alpha e^{i\sigma t}$$

$$= A(x, y) \cos (\sigma t - \theta(x, y)),$$
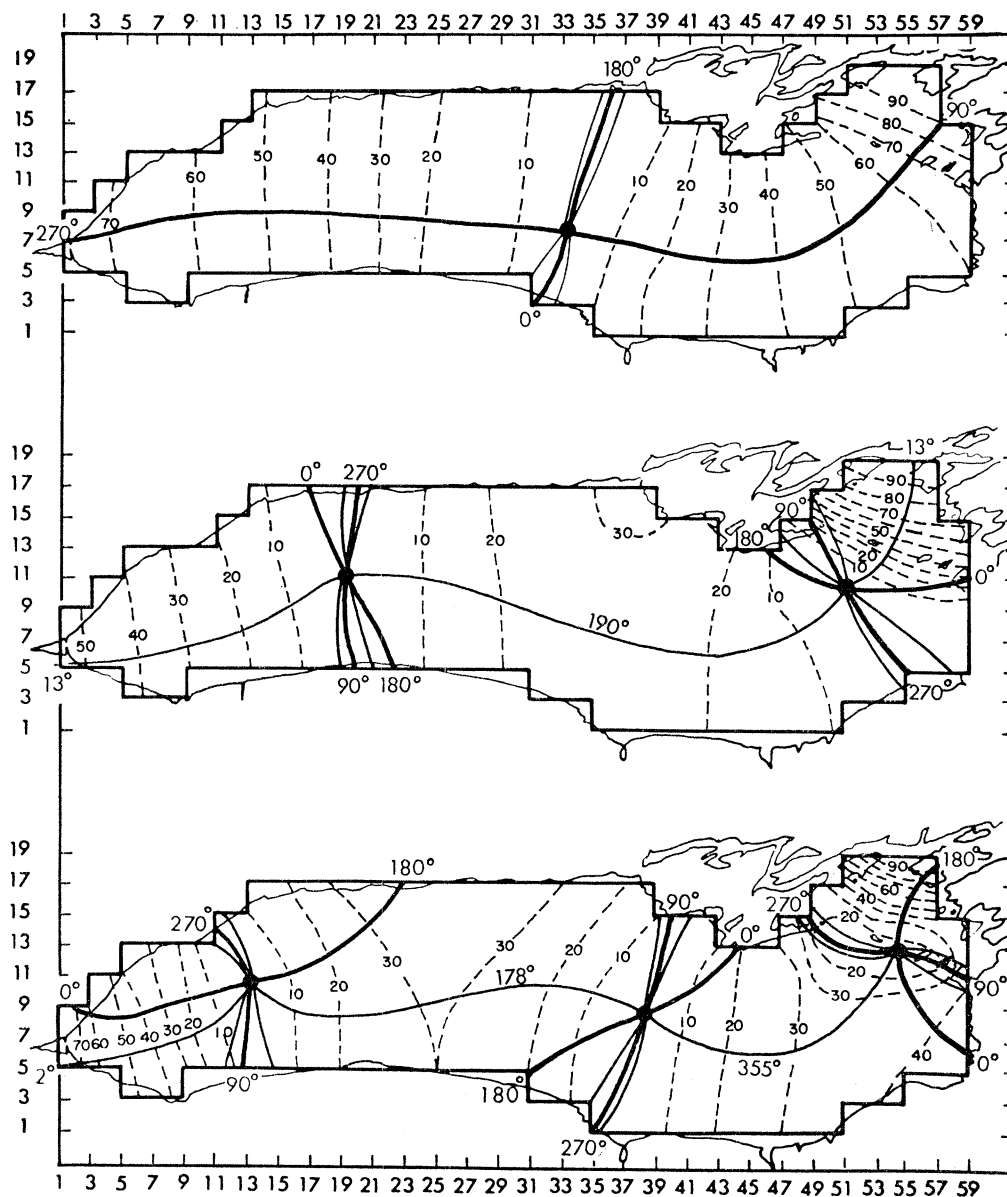
FIGURE 5. The first, second, and third normal modes for Lake Ontario.

where $A(x,y)$ is the amplitude and $\theta(x,y)$ is the phase of high water. The high water propagates in the direction of increasing $\theta(x,y)$ $(0 < \theta < 360°)$.

The gravest mode is shown at the top of figure 5. It consists of a single amphidromic point located slightly to the east of the centre of the basin around which the high water propagates in a positive sense of the horizontal plane (counter-clockwise sense). The amplitude of water level oscillation is always zero at the amphidromic point and increases away from it, towards the boundaries of the basin. The co-range lines are almost straight in the north–south direction indicating that rotation has only a small effect on the amplitude distribution around the basin. The counter-clockwise propagation of the phase of the lowest mode is in agreement with the behaviour of the lowest gravitational modes in basins rotating in the positive direction. The
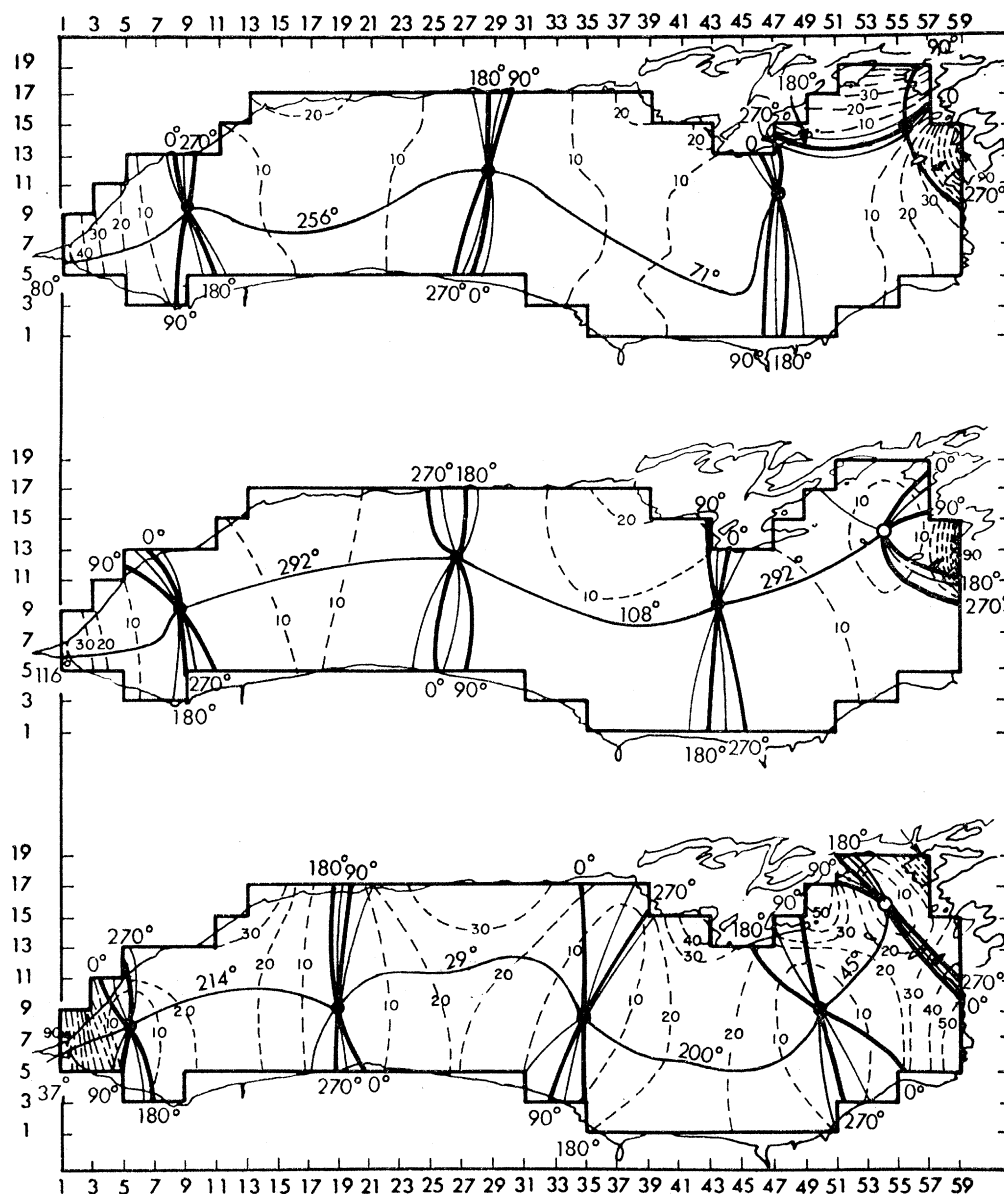
FIGURE 6. The fourth, fifth, and sixth normal modes for Lake Ontario.

second and third gravitational modes have two and three positive amphidromic systems respectively. The first three modes in figure 5 may be viewed as rotating counterparts of the lowest three non-rotating longitudinal modes presented in figure 3. In all of these modes, the oscillation amplitude is more pronounced in the northeastern part of the basin. The features of the lowest three gravitational modes presented here agree with those calculated by Hamblin (1972).

The fourth gravitational mode in our calculations has a period of 1.87 h and its structure consists of four positive amphidromic points as indicated in the top panel of figure 6. The non-rotating transverse oscillation in the eastern basin becomes a positive amphidromic system when rotation is included. This mode appears to have been missed by Hamblin (1972) in his calculations. This is also indicated in table 5 where no period value is given in the column corresponding to Hamblin's calculations.

The fifth gravitational mode which exhibited a longitudinal oscillation in the eastern basin in the non-rotating case consists of one amphidromic point with clockwise (negative) propagation in the eastern basin and three positive amphidromic points to the west of it. The sixth gravitational mode has again a negative amphidromic point in the eastern end of the basin with four positive amphidromic points to the west of it. The features of the fifth and sixth gravitational modes calculated here agree well with those identified as the fourth and fifth gravitational modes by Hamblin.

The preceding description concludes the properties of some of the lowest gravitational modes in Lake Ontario. We next examine briefly the gravitational modes in Lake Superior.
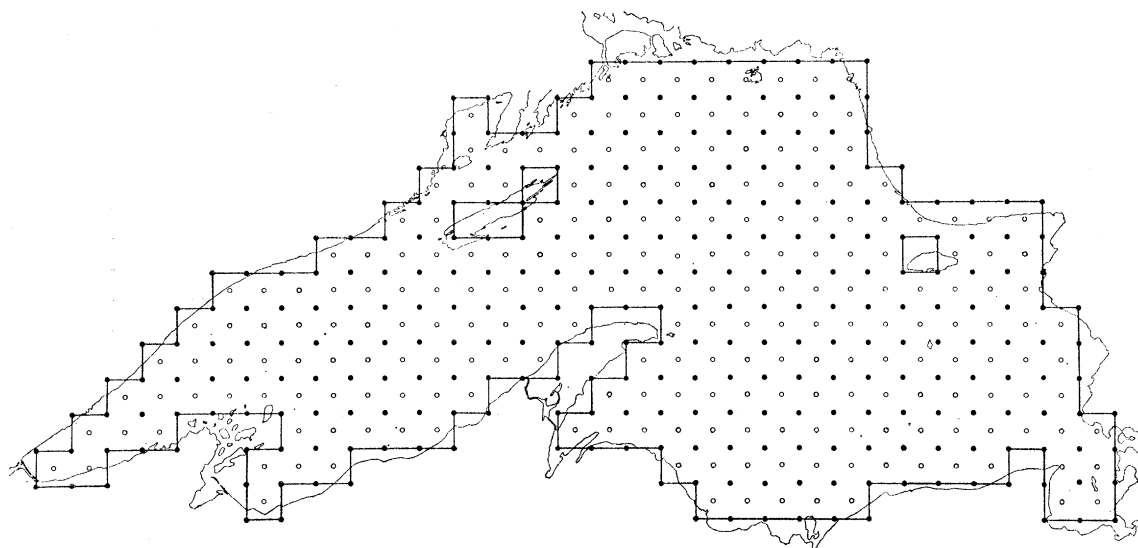

FIGURE 7. Numerical grid on Lake Superior.

(ii) *Lake Superior*

Bathymetric data for Lake Superior have been obtained from a chart compiled by R. J. Ristic at the Center for Great Lakes Studies. A grid interval between any two successive ϕ or ψ points of 60 000 ft (*ca.* 18.29 km) is used as in figure 7. The choice of the above grid interval gives a total of 160 interior points for ψ and 227 points for ϕ.

In table 6 are presented the periods of the lowest seven gravitational modes without rotation along with the available periods from the channel calculation of Rockwell (1966). It is again seen

that the two dimensional calculation increases the period of oscillation over the corresponding channel calculation.

Structures of the lowest six non-rotating gravitational modes are presented in figures 8, 9, and 10. The first mode exhibits a single nodal line. Maximum water level fluctuation on the western end is about twice that on the eastern end. The second mode, with two nodal lines, has maximum water level fluctuation on the ends of the basin and less than a third this value in the centre. Even though these oscillations take place mainly along the longitudinal axis of the lake as would be the assumption in a channel calculation, the two dimensional shape of Lake Superior reflects itself in the asymmetric distribution of water levels on either side of the axis. This is even more apparent
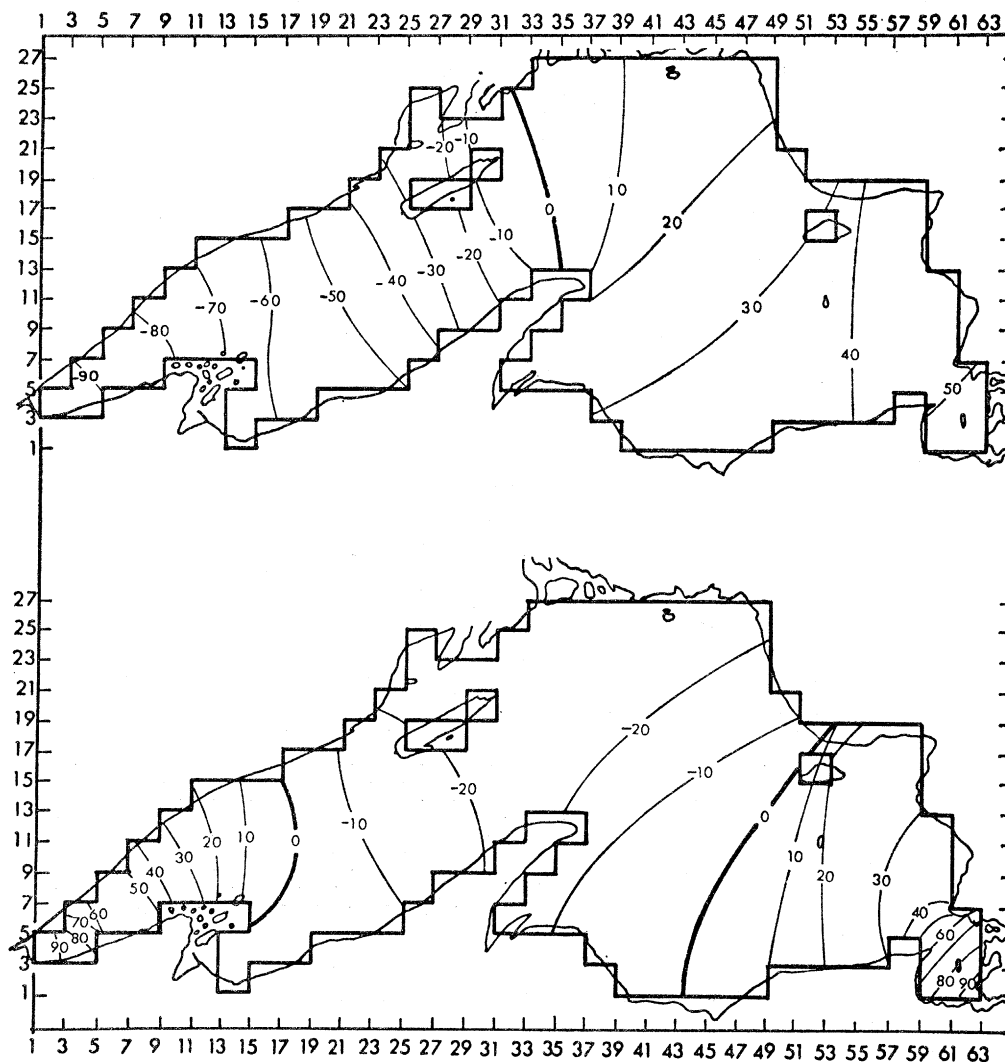
FIGURE 8. The first and second non-rotating normal modes for Lake Superior.

in the higher modes. The water level fluctuation between the nodal lines in the third mode reaches a maximum value only on the shoreline (in the Apostle Island Region and Keweenaw Bay) instead of maintaining the same value across the breadth of the lake. A channel calculation cannot represent this behaviour. The same effect occurs in the fourth mode which because of its transverse nature in the east-central part of the basin was missed in Rockwell's (1966) channel

calculation. The fifth mode has four nodal lines (as did the fourth) and is identified with the fourth mode of the channel calculations because of its predominantly longitudinal character. The sixth mode has essentially five nodal lines, one being interrupted by the Keweenaw peninsula. There is a large water level fluctuation in the Apostle Island Region and near Thunder Bay on the north side of the basin. The seventh two dimensional mode is identified with the fifth channel mode based on its longitudinal structure (this figure is not included here).
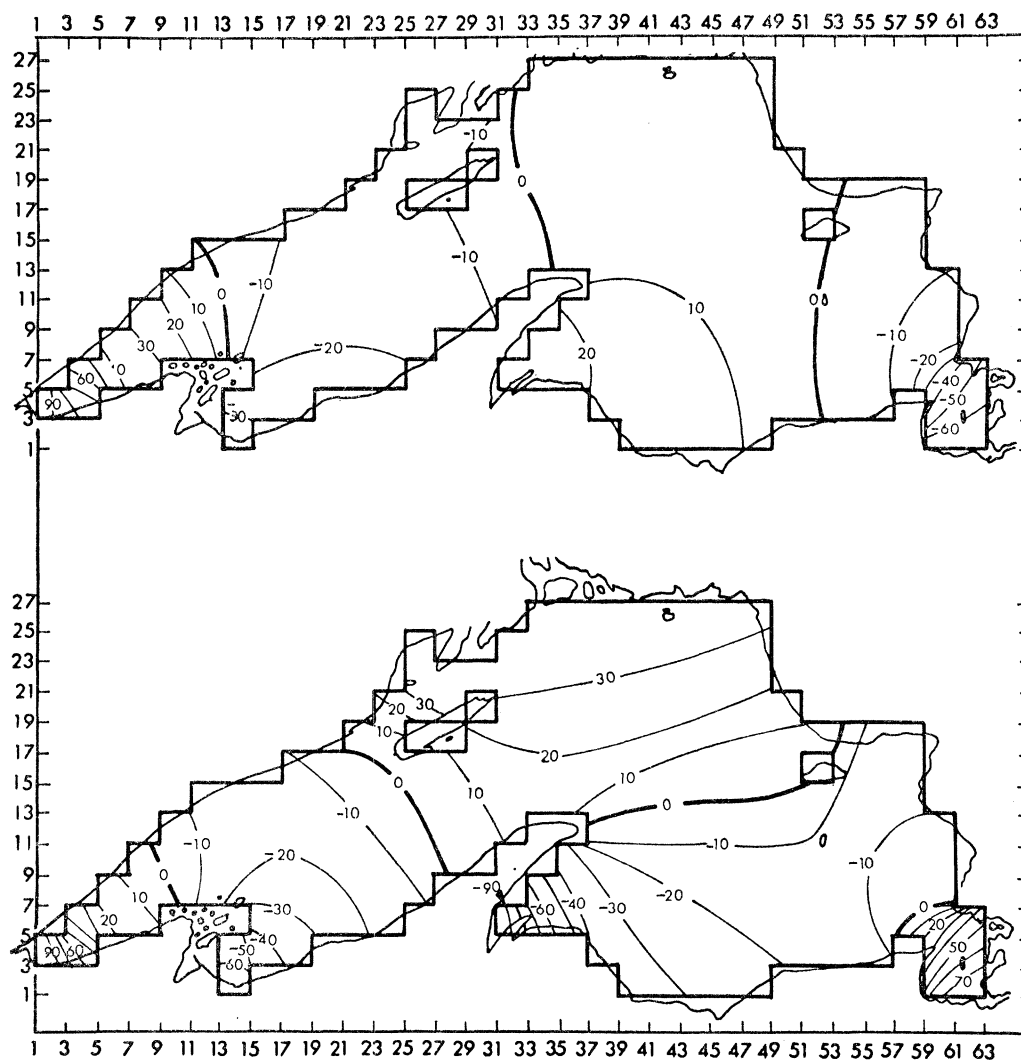
FIGURE 9. The third and fourth non-rotating normal modes for Lake Superior.

The modal characteristics with rotation are calculated by taking again the lowest 80 basis functions ϕ_α and ψ_α. In table 7, the periods of the lowest six gravitational modes are presented. It is seen again that period change due to rotation is quite negligible in the Lake Superior case also. It is attributable to the fact that the actual period value of close to 8 h is relatively small compared to the local inertial period of 16 h.

The structures of the lowest six gravitational modes are presented in figures 11, 12 and 13, in terms of amplitude and propagation of the phase of high water. The lowest mode has a single positive amphidromic point located approximately in the centre of the basin. The second, third

TABLE 6. NON-ROTATING PERIODS OF OSCILLATION FOR SOME OF THE GRAVITATIONAL MODES
OBTAINED FROM THE TWO DIMENSIONAL THEORY AND FROM THE CHANNEL THEORY

| | period/h | | |
mode	two dimensional result	channel result	percentage difference
1	7.83	7.19	8.9
2	4.42	4.30	2.8
3	3.75	3.29	14.0
4	3.16	—	—
5	2.96	2.84	4.2
6	2.57	—	—
7	2.40	2.24	7.1
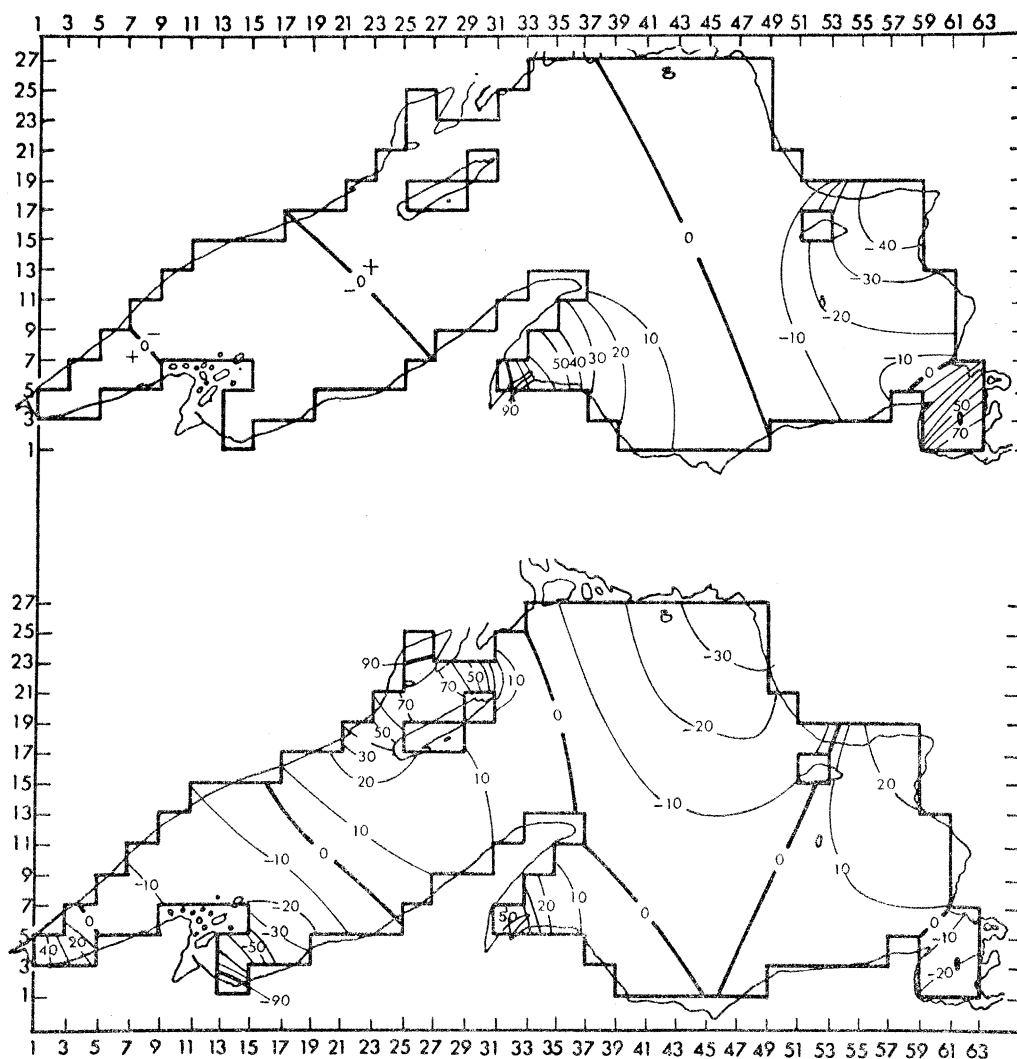
FIGURE 10. The fifth and sixth non-rotating normal modes for Lake Superior.

and fourth modes have respectively two, three and four amphidromic systems around all of which the phase propagates in a positive sense. The fifth mode again has four amphidromic systems. The two in the western end of the lake and the one in the eastern end are positively propagating systems, while the amphidromic system located in the middle of the lake approximately along the east–west section 44, is a negatively propagating amphidromic system. The sixth gravitational mode has six amphidromic systems, five of which are positive and the sixth

TABLE 7. PERIODS OF THE LOWEST SIX GRAVITATIONAL MODES IN LAKE SUPERIOR
WITH ROTATION

mode	period/h
1	7.86 (Platzman's calculation 7.84)
2	4.45
3	3.76
4	3.17
5	2.94
6	2.58
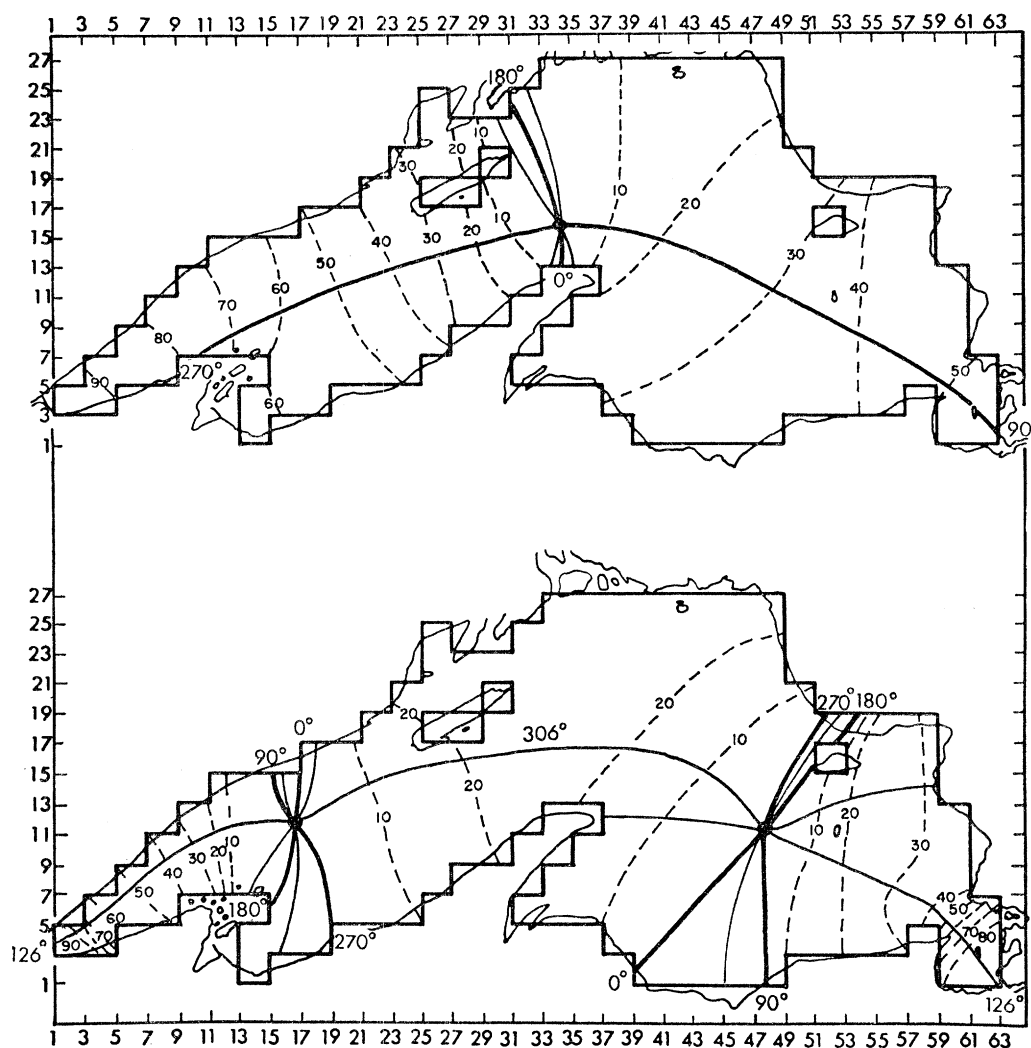
FIGURE 11. The first and second normal modes for Lake Superior.

one is a negatively propagating system with its amphidromic point located just east of the mouth of Keweenaw Bay. (See Mortimer & Fee 1976, p. 59 for the 7th and 8th modes.) We will consider verification of these gravitational mode characteristics in a later section.
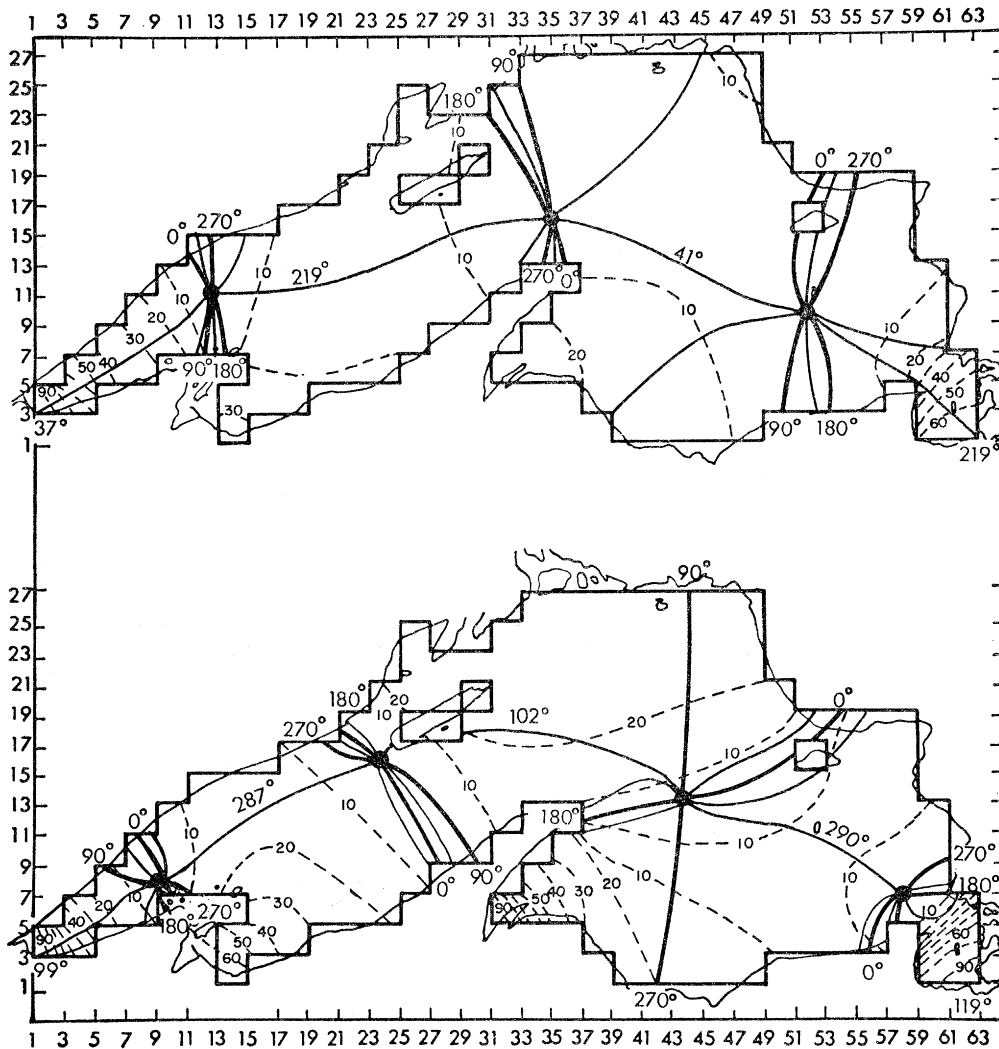

FIGURE 12. The third and fourth normal modes for Lake Superior.

(b) Rotational modes

(i) *Lake Ontario*

For Lake Ontario, 40 rotational modes with periods ranging from 52 h to some 14 years were calculated. It was found that the convergence of roots corresponding to rotational modes as the size of the coefficient matrix (3.23) is increased is more complicated than for gravitational modes. At successively higher truncations roots appear with larger and smaller values than the largest and smallest roots for the previous truncation. In this sense it is not possible to speak of the lowest rotational mode as one does the lowest gravitational mode. The most important rotational modes are those with the largest space scale. Since it is not possible to determine the space scale of these rotational modes by merely examining the periods, the structures of all 40 modes in Lake Ontario were examined and two were selected for study here.

Streamlines of the mass transport field at $\sigma t = 0$ and $\sigma t = \frac{1}{2}\pi$ are presented in figure 14 for the rotational mode with a period of 229 h (about 10 days). At $\sigma t = \pi$ and $\sigma t = \frac{3}{2}\pi$ the magnitudes of the stream function are the same as at $\sigma t = 0$ and $\sigma t = \frac{1}{2}\pi$, respectively; but the sign is reversed. This mode is of interest because a previous calculation by Hamblin (1972) indicated a rotational mode in Lake Ontario with a period of 236 h which was compared to the cubic rotational mode of an elliptic paraboloid. Possible differences in the origin of phase and comparison of streamlines to velocity vectors make direct comparison difficult but the general features of the 236 and 229 h
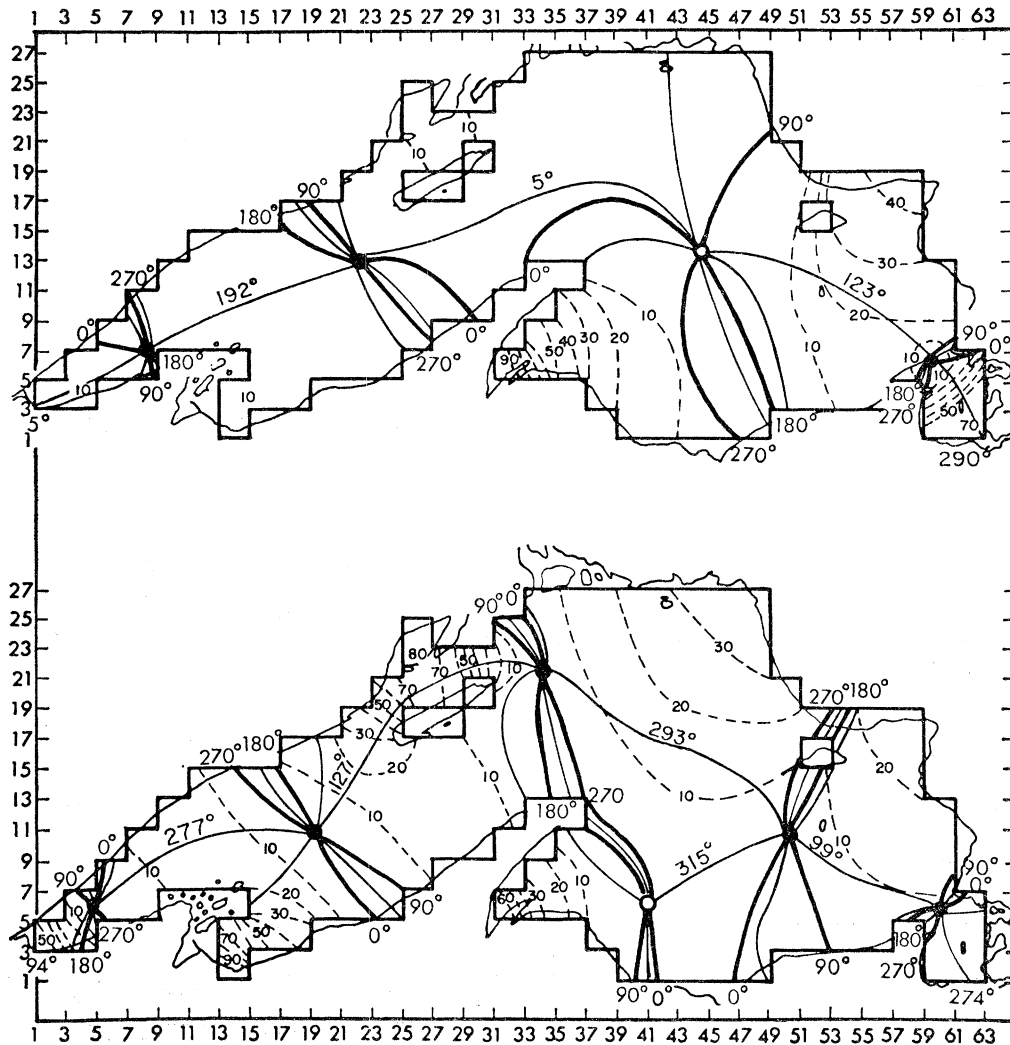

FIGURE 13. The fifth and sixth normal modes for Lake Superior.

modes are similar. At $\sigma t = 0$ the centre of the basin is dominated by clockwise current propagation (higher values of stream function lie to the right of the current direction) giving rise to easterly flow along the northern shore and westerly flow along the southern shore. In the western part of the basin a counterclockwise gyre forces the current northwards when it meets the westward flow along the southern shore. The clockwise propagation in the north and counterclockwise propagation in the south cause a westward flow in the central part of the eastern basin. Where this flow meets the clockwise propagation in the central basin, southward flow results.

At $\sigma t = \frac{1}{2}\pi$ the main features are the counterclockwise gyre in the eastern basin and the clockwise cell in the east–central region. The current is southward where they meet, eastward along the southern shore of the eastern basin and westward along the southern shore of the central region. In the far western basin, clockwise flow predominates.

A far more interesting mode with a period of 464 h (about 20 days) is shown in figure 15. At $\sigma t = 0$ a clockwise cell predominates in the western half of the lake with counterclockwise motion
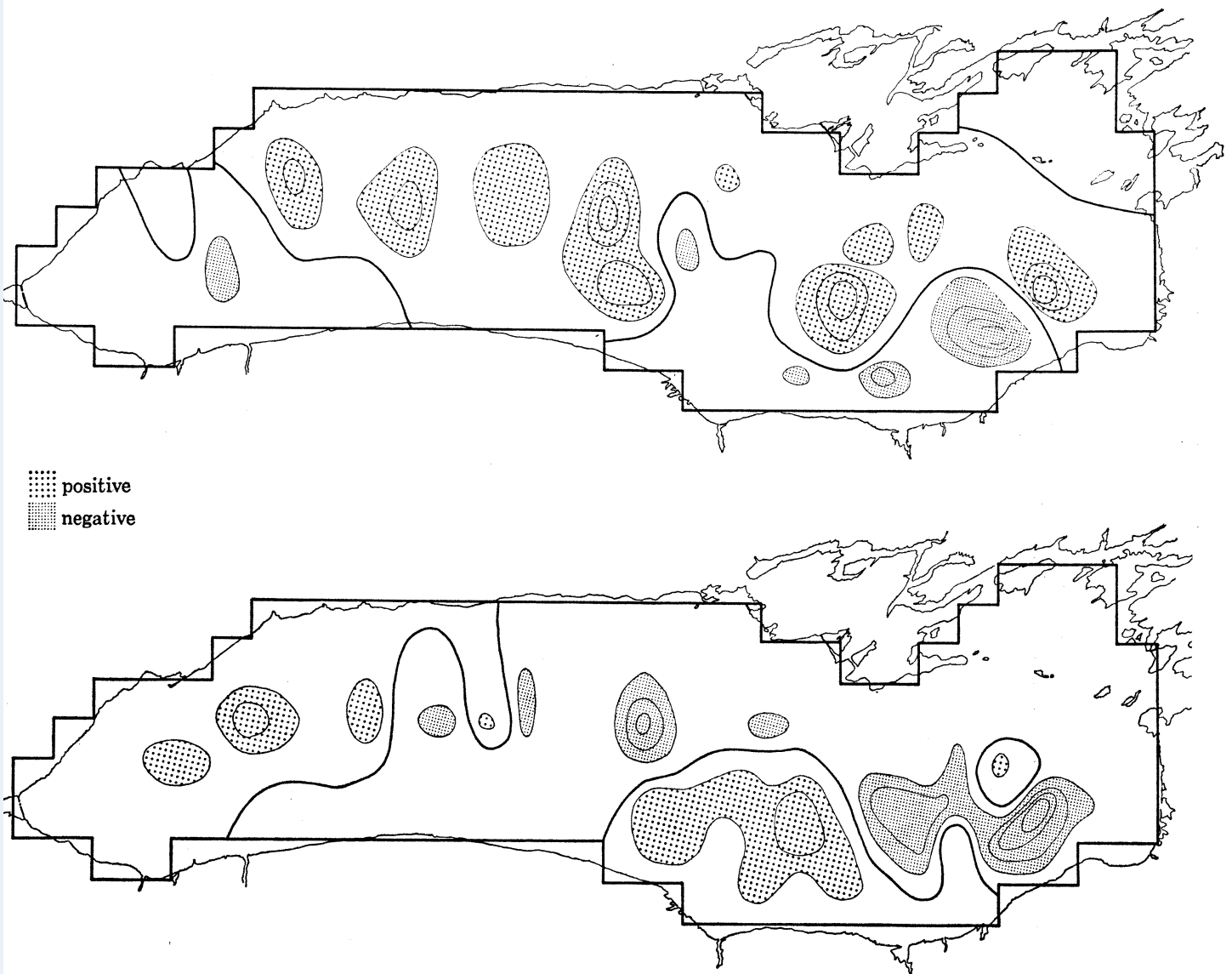

::::: positive
::::: negative

FIGURE 14. Rotational normal mode with a period of 229 h for Lake Ontario.

in the eastern half. The most vigorous currents are eastward in the northern part of the central basin and southwestward in the centre of the lake. When $\sigma t = \frac{1}{2}\pi$, the counterclockwise cell extends across the northern half of the basin from end to end and the clockwise cell has moved to the southern half of the basin. Strong currents are established from west to east in the central parts and from east to west along the northern and southern shores. The counterclockwise motion of the two gyres around the centre of the basin and the accompanying counterclockwise rotation

of the current vectors more closely match the circulation pattern in the cubic rotational mode of the elliptic paraboloid than the features of the 229 h mode, though the period is not as close. At $\sigma t = \frac{3}{2}\pi$ the stream lines will very closely resemble the steady-state circulation of the lake when subjected to wind stress from the west with westward flow along the shores and return flow in the centre. This mode has the largest space scale of all rotational modes calculated in Lake Ontario and is expected to be important in the low-frequency response of the lake.
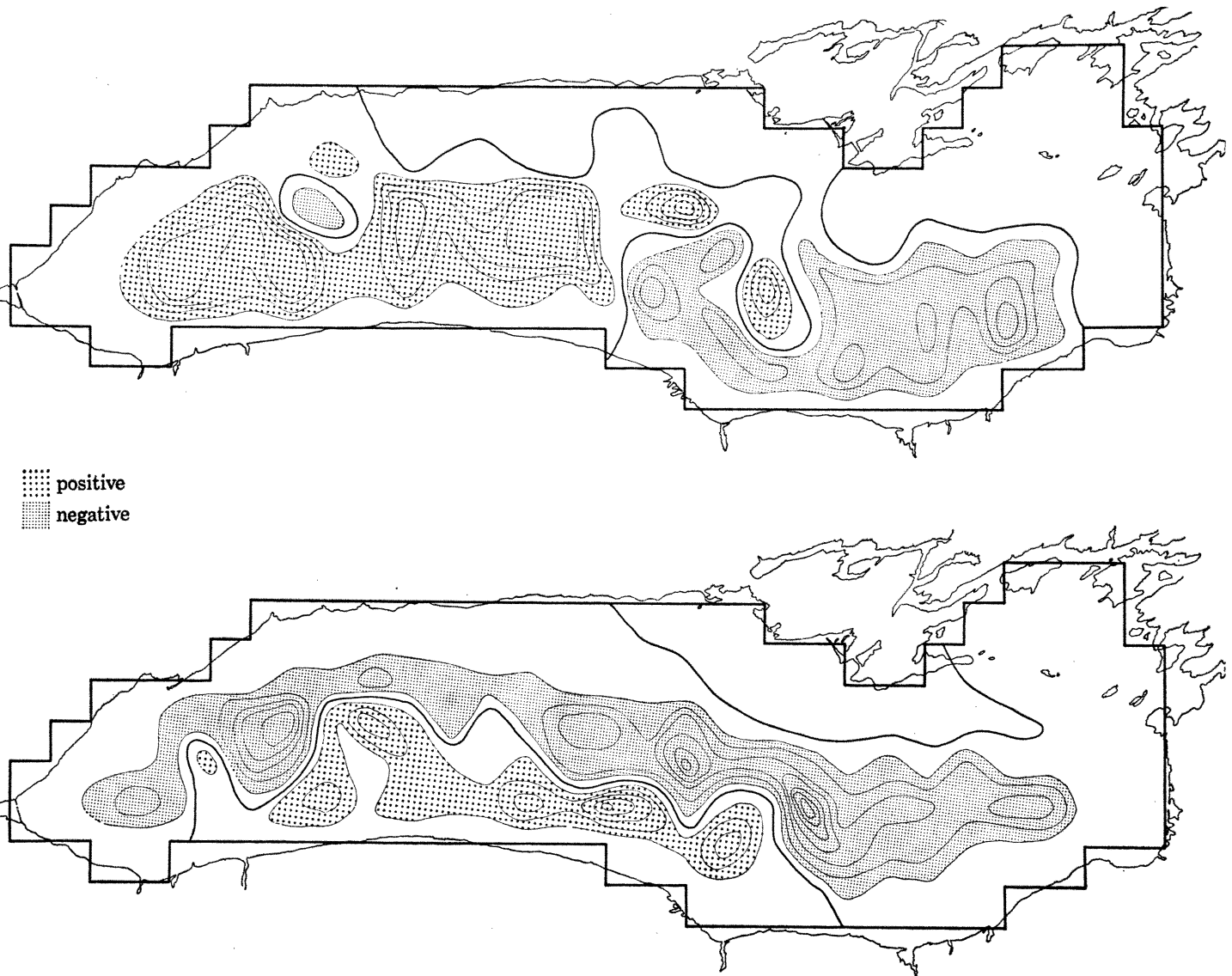
positive
negative

FIGURE 15. Rotational normal mode with a period of 464 h for Lake Ontario.

(ii) Lake Superior

Forty rotational modes with periods from 79 h to several thousand years were calculated. Examination of the structures of these modes indicates that the complex topography of Lake Superior tends to disorganize the cell patterns to such a degree that no modes with as large a space scale as the 464 h mode in Lake Ontario could be found. The most organized mode with a reasonably large space scale is presented in figure 16. This mode has a period of 169 h (about

7 days) and consists essentially of two large clockwise cells enclosing a counterclockwise cell in the centre of the eastern basin at $\sigma t = \frac{1}{2}\pi$. If one can visualize the pattern at $\sigma t = 0$ as four pairs of counter-rotating gyres aligned in a north–south direction, with the clockwise part of each pair
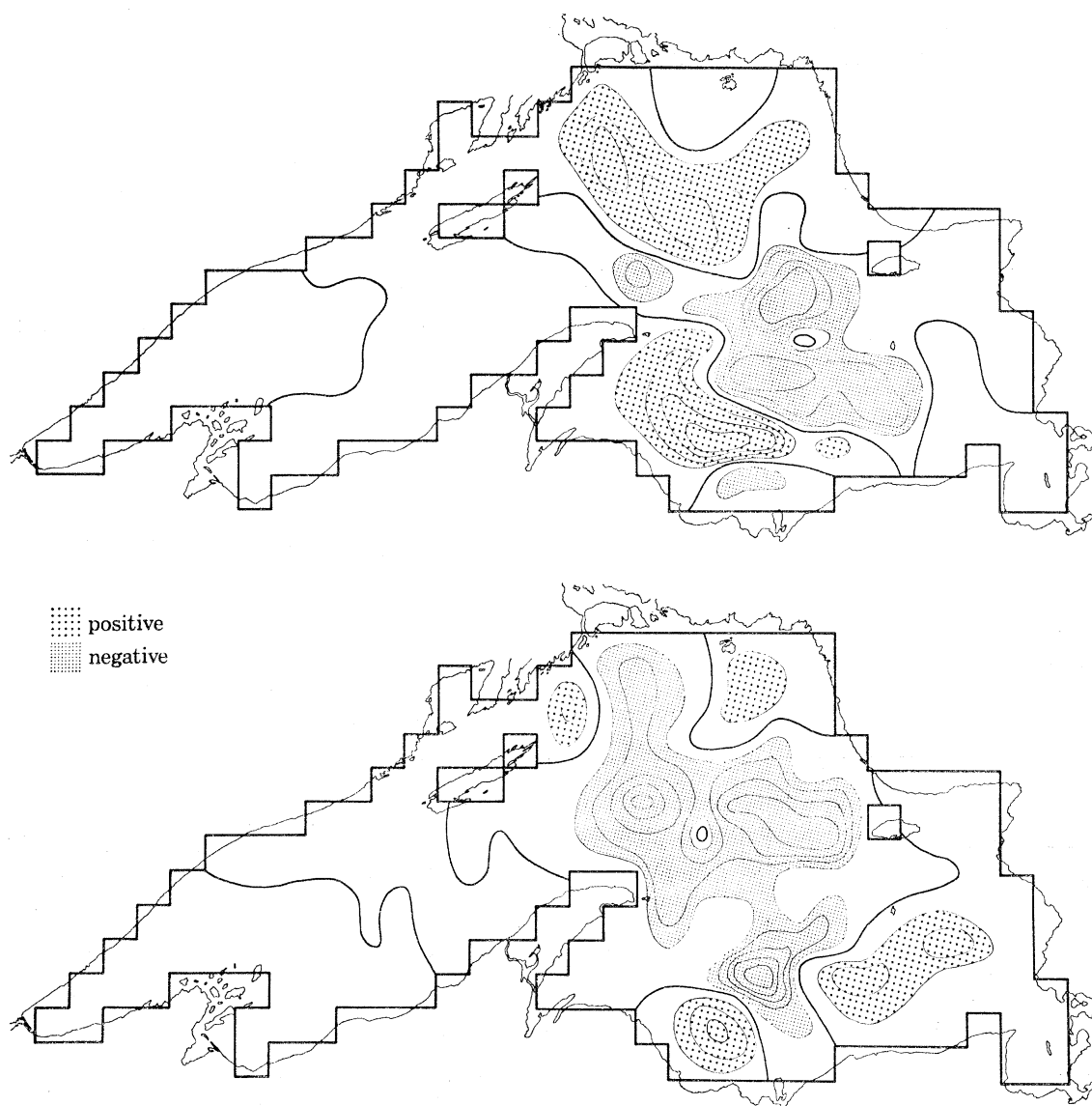

FIGURE 16. Rotational normal mode with a period of 169 h for Lake Superior.

closest to the shore so that all four counterclockwise cells occupy the central part of the basin, then the structure at $\sigma t = \frac{1}{2}\pi$ indicates that the northwest and southeast sets of cells are travelling in a counterclockwise circle while the northeast and southwest pairs travel in clockwise circles. This eight cell pattern resembles a higher order rotational mode in an elliptic paraboloid.

Figure 17 represents a rotational mode in Lake Superior with a period of 441 h and is included to indicate the complexity of most of the rotational modes in Lake Superior. At $\sigma t = 0$ there seem to be two separate areas of activity, one in the north–central part of the lake, and the other in the east, which are not too complicated in themselves, but at $\sigma t = \frac{1}{2}\pi$ the two areas have merged and

the cell pattern extends over the entire east–central part of the basin. This mode is representative of many of the rotational modes in Lake Superior in that the number of cells and their spatial distribution change significantly from $\sigma t = 0$ to $\sigma t = \frac{1}{2}\pi$.
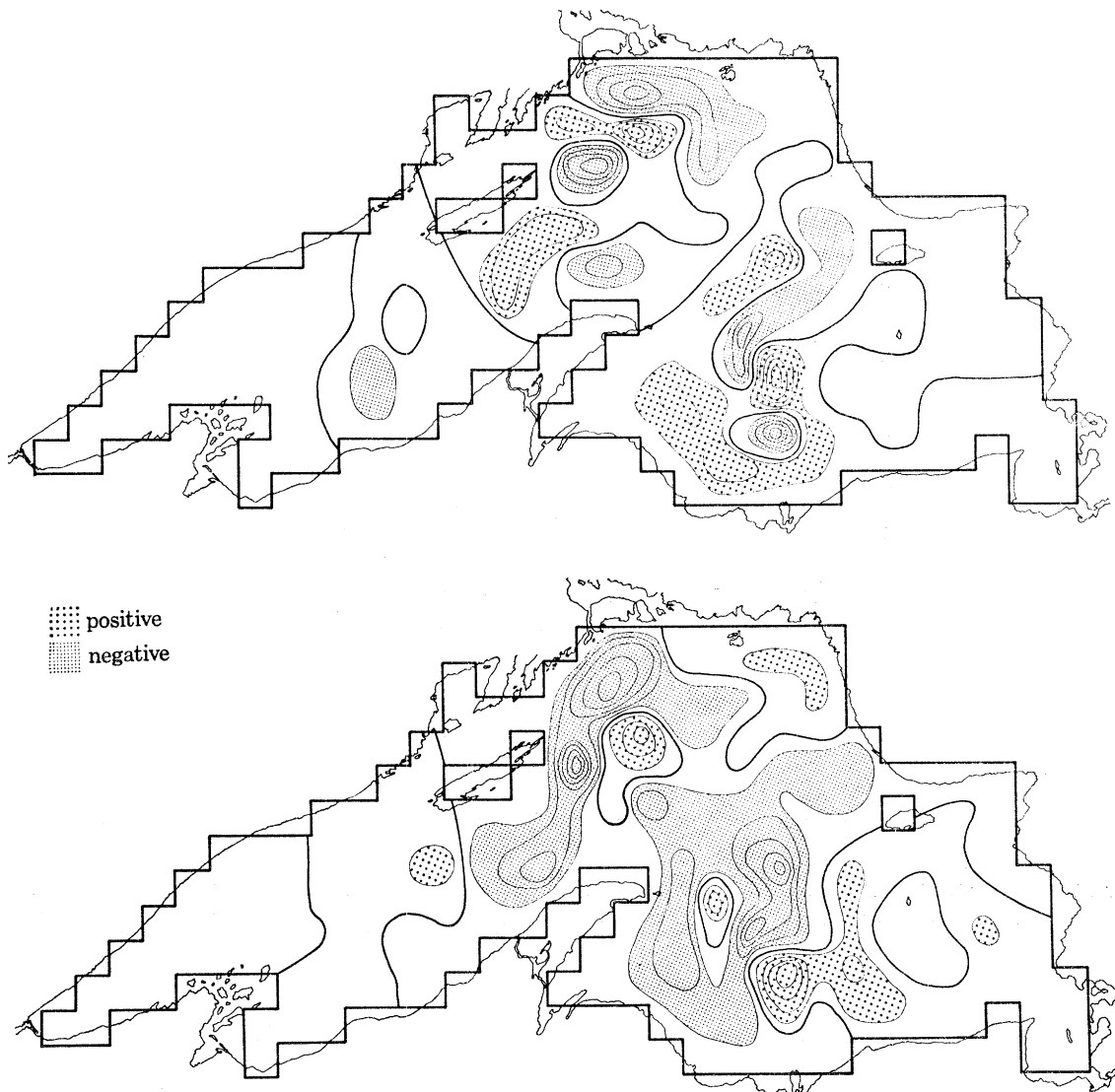

positive
negative

FIGURE 17. Rotational normal mode with a period of 441 h for Lake Superior.

7. VERIFICATION OF THE RESULTS

Analysis of water level data in Lake Ontario has been confined to only a few published reports that deal with a small number of stations over short periods of time. Recently, however, statistical spectral analyses of the water level from several stations over month-long periods have become available (P. W. Sloss 1974, personal communication). The spectrum presented in figure 18 is for hourly water level data at Sackett's Harbor on the northeastern shore of Lake Ontario during the month of October in 1972.

The lake is homogeneous in this season and usually subject to significant atmospheric forcing.

92   D. B. RAO AND D. J. SCHWAB

Also, the first three gravitational modes in Lake Ontario exhibit large enough amplitude at Sackett's Harbor to be readily detected. The spectral peaks at 05 h 00, 03 h 12, and 02 h 30 are within a few percent of the calculated periods for the first three modes. Since most of the water level data taken on Lake Ontario are hourly, verification of the higher modes is impossible.
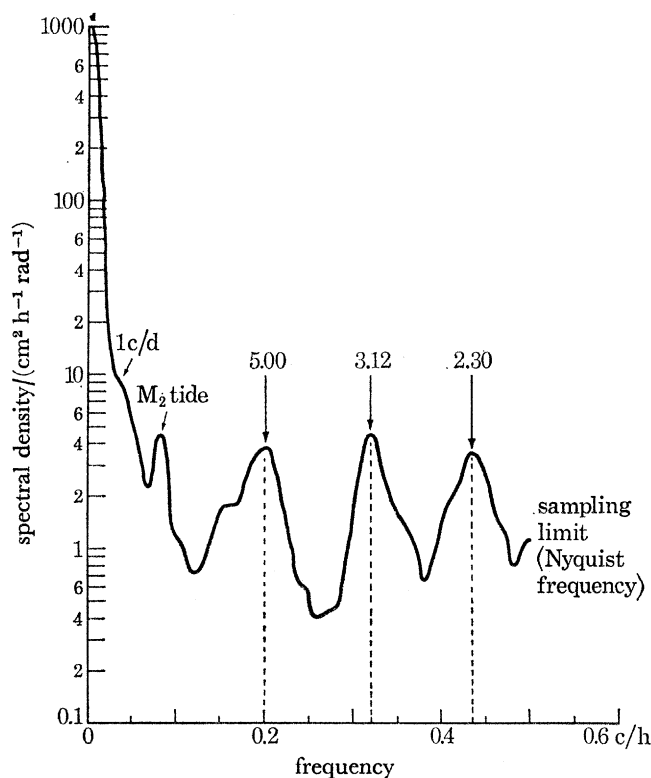

FIGURE 18. Power spectrum of hourly water level data from Sackett's Harbor on Lake Ontario.

TABLE 8. COMPARISON OF OBSERVED AND CALCULATED PERIODS OF THE LOWEST FIVE GRAVITA-TIONAL MODES IN LAKE SUPERIOR. OBSERVED VALUES ARE TAKEN FROM MORTIMER & FEE (1976)

| | period/h | | percentage |
mode	observed	calculated	difference
1	7.89	7.86	0
2	4.84	4.45	8
3	3.80	3.76	1
4	3.37	3.17	6
5	3.02	2.94	3

Verification of the theoretical calculations is less difficult for the gravitational modes of Lake Superior for which extensive analyses of water level data were made by Mortimer & Fee (1976). By spectral analysis of water level data from ten stations, Mortimer & Fee calculated the periods of several free modes and their phase propagation along the boundary of the lake. In table 8 are presented the periods of the lowest five modes determined from the spectral analysis and from the theoretical calculations. The agreement between computed and observed periods is very good. Errors of 8 and 6 % associated with the second and fourth modes can be attributed in part

to the fact that in Mortimer & Fee's analysis, the peaks corresponding to even harmonics are not as high as those for odd harmonics.

Mortimer & Fee (1976) speculated on the two dimensional structures of the first five gravitational modes. The structure of each mode was synthesized from data on propagation of the phase of high water obtained from spectral analyses. Co-tidal lines were drawn in the lake in such a manner that they are consistent with the calculated phase values on the boundary. With only ten points around the periphery of the lake, construction of the modal structure in the

(a) band no. 76
≈ 1st mode
frequency 3.04 c/d
period 7.89 h

(b) band no. 214
≈ 2nd mode
frequency 4.95 c/d
period 4.84 h

(c) band no. 158
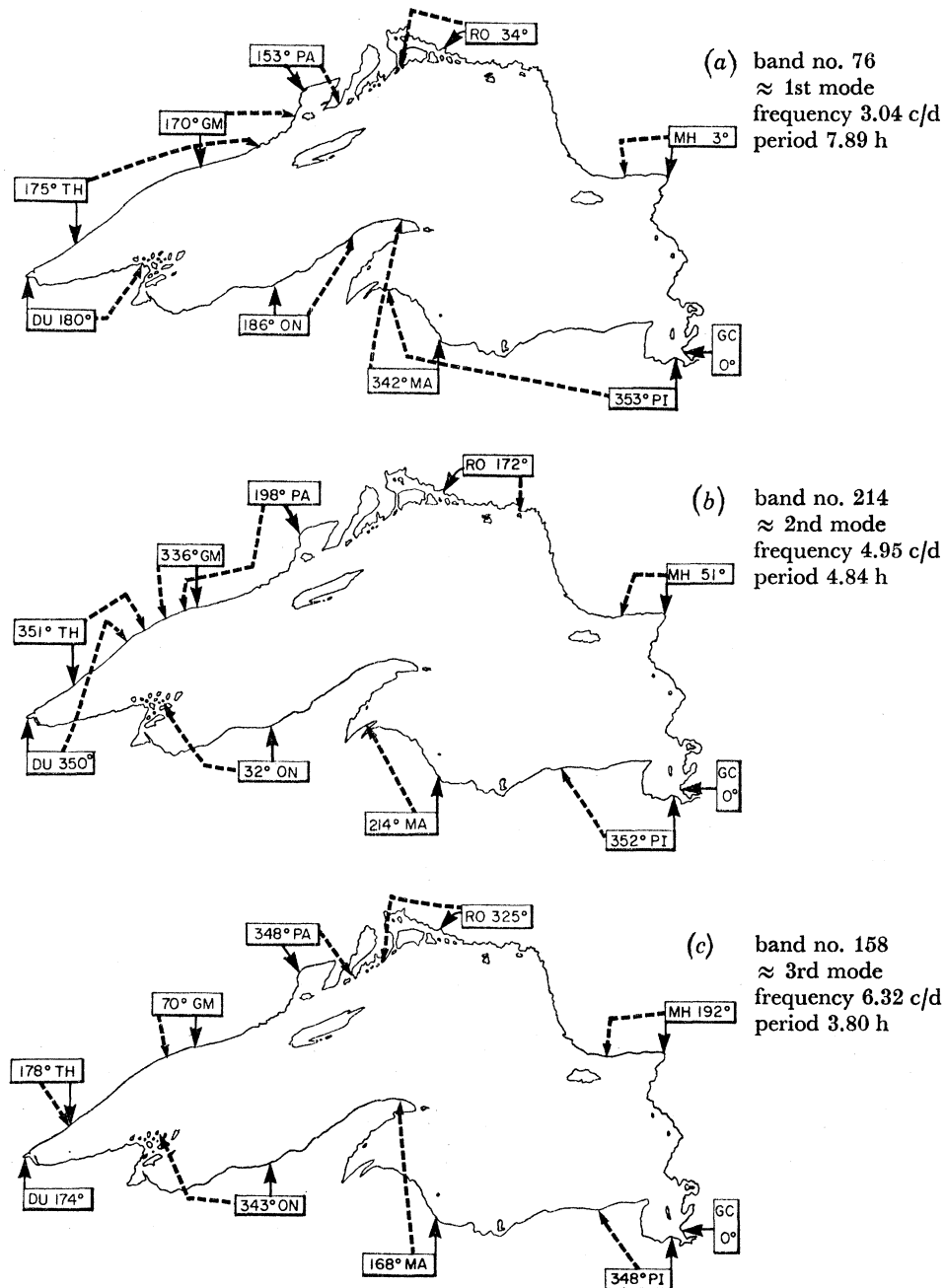≈ 3rd mode
frequency 6.32 c/d
period 3.80 h

FIGURE 19. Comparison of observed (solid) and calculated (dashed) locations of occurrence of phase in Lake Superior for the first, second and third normal modes. Phase angles are relative to 0° at GC.

interior of the lake becomes rather difficult; particularly as one proceeds to the higher modes. In figures 19 and 20, we have shown simply the phase of high water for the lowest five gravitational modes obtained from Mortimer & Fee (1976, table 8) and from our calculations. In these diagrams we have blotted out the structures of the modes. (The reader may refer to figures 11, 12 and 13 for the theoretically calculated structures.)

Figure 19 makes the comparison for the lowest three gravitational modes. The speculated structures of Mortimer & Fee are almost identical to the structures of these modes as calculated here. Unbroken arrows indicate the points on the shore where a certain 'observed' value of the phase angle (indicated inside box) occurs. Broken arrows indicate the point at which the same phase angle is predicted from our calculations.
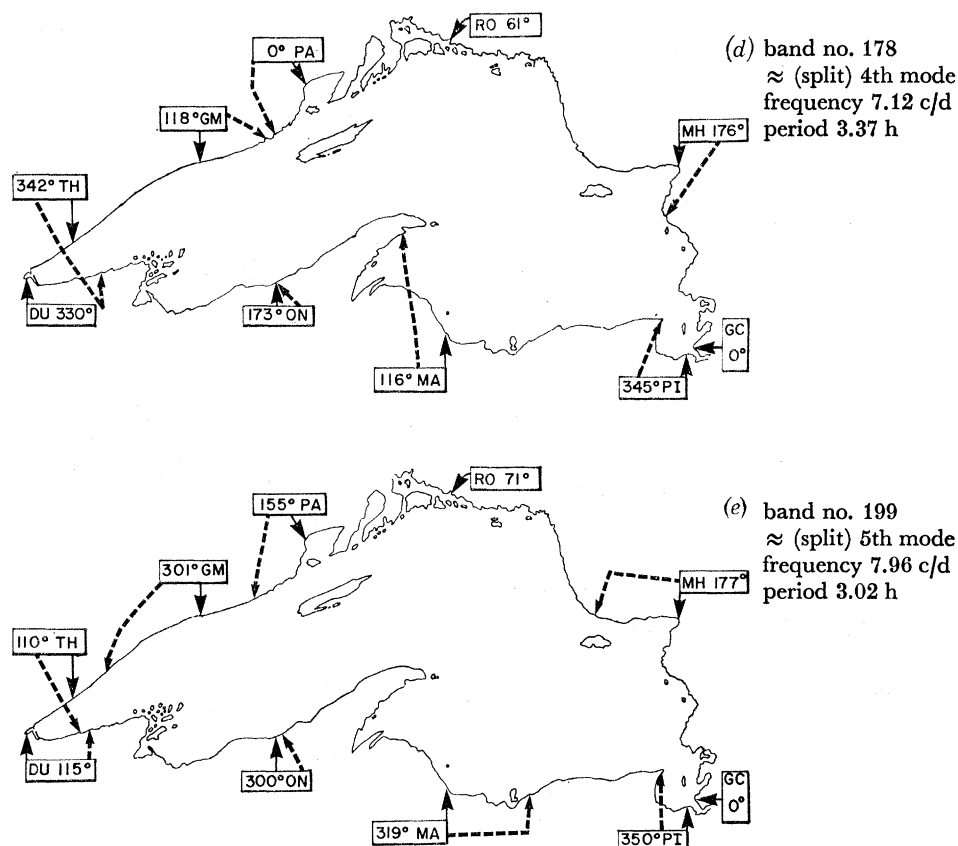

FIGURE 20. Comparison of observed (solid) and calculated (dashed) locations of occurrence of phase in Lake Superior for the fourth and fifth normal modes. Phase angles are relative to 0° at GC.

Consider the lowest gravitational mode (top panel of figure 19). The agreement between theory and observation may look poor particularly at Point Iroquois (PI) and Marquette (MA). The actual difference in phase exactly at PI and MA are 7° and 14°, respectively. However, it should be noticed that the phase changes very slowly along the southern boundary of eastern Superior, the total change in phase angle being approximately 20°. A similar situation prevails on the northern boundary of western Superior between Two Harbors (TH) and Grand Marias (GM) with a total change in phase of about 5°. Hence, any minor error either in the observed data or in the numerical procedure may appear to produce a large shift of the point where a certain value of phase is occurring. If the theoretical model is used to read off the phase angles at

points where these angles are available from Mortimer & Fee's analysis, the results would appear as shown in table 9.

The other differences in the location of a point where a given phase angle occurs according to theory and observation are within a distance of a grid square. If one ignores the data from Duluth (DU) and Rossport (RO), both of which are considered to be of rather poor quality, the overall agreement between theoretical and observational phase angles is quite satisfactory, for the lowest five modes (and for the 8th mode (Mortimer & Fee 1976. p. 59)).

TABLE 9. COMPARISON OF OBSERVED AND CALCULATED PHASE ANGLES FOR THE PROPAGATION OF THE LOWEST GRAVITATIONAL MODE IN LAKE SUPERIOR. OBSERVED VALUES ARE FROM MORTIMER & FEE (1975)

location	theoretical	observed	difference
Gros Cap (GC)	0†	0†	0†
Michipicoten (MH)	2	3	1
Rossport (RO)	18	34	16
Port Arthur (PA)	172	153	19
Grand Marias (GM)	179	170	9
Two Harbors (TH)	179	175	5
Duluth (DU)	180	180	0
Ontanagon (ON)	182	186	4
Marquette (MA)	356	342	14
Point Iroquois (PI)	0	353	7

† Following Mortimer & Fee, the phase at Gros Cap is arbitrarily taken as zero.

The effect of friction was ignored in the calculations here. The fundamental difficulty in assessing the effect of friction in a lake is that no procedure exists by which the turbulent frictional forces can be introduced into the dynamical equations in a rigorous manner. A heuristic procedure commonly adopted is that friction may be represented through a linear skin-friction law: It may be shown, for such a law, that to the first order friction does not modify the period but introduces a decay (so long as the coefficient of friction is small compared to the frequency of oscillation) (see, for example, Dantzig & Lauwerier 1960). The period of oscillation is changed (increased) when second order effects are considered. In an analysis of the effects of friction on the oscillations in Lake Erie, Platzman & Rao (1964) concluded that a linear friction law would increase the period of the lowest mode by about 1%. This analysis is for a one-dimensional channel system. Such a conclusion may still be valid even with rotation. The small period increase due to friction would result in a slight retardation in the propagation of the phase of high water around the basin. Hence, even in Lake Erie which is the shallowest of all the Great Lakes, the effect of friction on the normal modes is not very large. Lakes Ontario and Superior are deeper than Lake Erie and consequently the characteristics of the normal modes presented above will not be affected significantly by friction. Such a conclusion is confirmed by the small differences between the observed and calculated results presented above.

The rotational modes are of such long periods, it is difficult to verify them from observational data, particularly so from water level data in view of the nearly non-divergent character of these modes. A careful analysis of current meter data might help in resolving some of the rotational modes. Unfortunately, however, the stratification of the lakes changes significantly over the period of time necessary to take data in order to make any meaningful analyses for most of the rotational modes.

8. Conclusion

The problem of free oscillations in an arbitrary enclosed water body on a rotating earth has been solved by an application of numerical procedure to the analytical theory developed by Proudman (1916). The procedure was applied specifically to two of the Great Lakes of North America – Lake Ontario and Lake Superior. The numerical calculations yield the periods and structures of several rotational and gravitational modes. In the case of Lake Superior, detailed comparisons between the theoretical calculations and observations for several gravitational modes showed very good agreement. Extension of these calculations to the rest of the Great Lakes as well as other major enclosed water bodies is now being carried out.

References

Dantzig, D. Van & Lauwerier, H. A. 1960 The North Sea Problem. IV. Free oscillations of a rotating rectangular sea. *Proceedings, Koninklijke Nederlandske Akademie Van Wetenschappen*, A **63**, 339–354.

Defant, A. 1961 *Physical oceanography*, vol. ii. 598 pp. London: Pergamon Press.

Defant, F. 1953 Theorie der Seiches des Michigansees und ihre Abwandlung durch Wirkung der Corioliskraft. *Archiv für Meteorologie, Geophysik und Bioklimatologie*, A **6**, 218–241.

Hamblin, P. F. 1972 Some free oscillations of a rotating natural basin. University of Washington, Dept. Oceanography, Ph.D. Thesis, 97 pp.

Longuet-Higgins, M. S. & Pond, G. S. 1970 Free oscillations of a fluid on a hemisphere bounded by meridians of longitude. *Phil. Trans. R. Soc. Lond.* A **226**, 193–224.

Loomis, H. G. 1973 A new method for determining normal modes of irregular bodies of water with variable depth. *Hawaii Inst. Geophys. Tech. Rept.* HIG-73-10, June 1973, 27 pp.

Mortimer, C. H. & Fee, E. J. 1976 Free surface oscillations and tides of Lakes Michigan and Superior. *Phil. Trans. R. Soc. Lond.* A, **281**, 1–61.

Platzman, G. W. 1972 Two-dimensional free oscillations in natural basins. *J. phys. Oceanog.* **2**, 117–138.

Platzman, G. W. 1975 Normal modes of the Atlantic and Indian Oceans. *J. phys. Oceanog.* **5**, 201–221.

Platzman, G. W. & Rao, D. B. 1964 The free oscillations of Lake Erie. *Studies on Oceanography* (Hidaka Volume), (ed. K. Yoshida), pp. 359–382. Tokyo Univ. Press.

Proudman, J. 1916 On the dynamical theory of tides. Part II. Flat Seas. *Proc. London Math. Soc.* ser. 2, **18**, 21–50.

Rao, D. B. 1965 Free gravitational oscillations in rotating rectangular basins. University of Chicago, Dept. Geophys. Sci., Ph.D. Thesis, 142 pp.

Rockwell, D. C. 1966 Theoretical free oscillations of the Great Lakes. *Proc. 9th Conf. Great Lakes Res., University of Michigan, Great Lakes Res. Div., Publ.* No. 15, pp. 352–368.